Politecnico di Milano

Scuola di Ingegneria Industriale e dell'Informazione
Corso di Laurea Magistrale in Ingegneria Fisica
Dipartimento di Fisica

Mid-InfraRed Tunable, Carrier-Envelope-Phase Stable, Pulsed Source

Relatore: Prof. Giacomo Claudio GHIRINGHELLI
Correlatore: Dr. Michael FÖRST

Tesi Magistrale di:
Luca Piovani
Matr. 771212

Anno Accademico 2013-2014

Ai miei genitori, sotegno e forza delle mie azioni.

Ringraziamenti

First of all I would like to thank all the people that were directly involved in the making of this experience, so Dr. Michael Först, in primis, that wisely assisted me during the whole process, Prof. Ghiringhelli and Prof. Cavalleri that gave me the opportunity of working in the Quantum Condensed Matter Dynamics group in Desy and were always very kind and willing to help. Alongside them I am really glad to have shared some time with lots of other special people in the MPSD group, especially Andrea, my OPA buddy, we spent a lot of good moments together, Matteo, my daily companion, we have had great discussions and fantastic dinners together, Alberto who was always there whether it was for yelling at us, mumbling with us or drinking with us. Also I'd like to thank Rashmi that helped me with the measurements and Roman that kindly shared his office with me and all of the other people, scientists and non, that friendly accepted me in the group.

Il primo speciale ringraziamento in italiano va sicuramente ai miei Nonni e Zii che da sempre mi accolgono, nutrono e confortano, nonché a Mamma, Laura e D. che riempiono la casa di strilla, dolcezze e peli.

Il mio pensiero più grande va poi a Chiara, gioia e cruccio dei miei giorni, che mi è stata vicina sempre e che pazientemente ha sopportato e supportato ogni mio difetto e incertezza durante questo lungo percorso.

Non posso non fare il mio più sentito grazie ai miei compagni di scorribande notturne Attu, Brio, Marchino, Tau e Toffa senza i quali le serate di studio/pes sarebbero state molto più produttive ma assolutamente molto meno piacevoli, grazie mille ragazzi. Ancora grazie a tanti amici che da sempre sono presenti nella mia vita e che mi accompagnano in ogni discussione, cena, impresa o bevuta: Daddy, Arca, Lio tra tutti. Volevo poi ancora ringraziare tutti i miei compagni di corso che negli anni mi hanno aiutato e con i quali ho condiviso tanti splendidi momenti, Maz con i suoi indispensabili suggerimenti, Maran e Andrea per il fantastico spritz e le magnifiche feste, Sha per la saggezza e la follia, Manuz, Gaia, Chiara, il Monti e Gabry per le serate di divertimento e gioia passate insieme.

Contents

List of Figures

Chapter 1

Introduction

1.1 Abstract

In the recent years growing attention has been paid in Mid-Infrared (Mid-IR) few cycle sources. These have been demonstrated to be capable of both driving and probing a vast multitude of low energy elementary excitations in molecules as well as in solids. Control over this processes is particularly fascinating in strongly correlated materials where even tiny changes in the crystallographic structure can lead to gigantic effects[1]. For this and many others applications[2] shot to shot reproducibility of the pulses' electric field both in frequency and phase is crucial. The difference frequency generation process between Near-Infrared (NIR) beams coming from Optical Parametric Amplifiers has been successfully exploited for long a time to generate intense Mid-IR field with almost transform-limited duration. The relative temporal offset of the carrier of a Mid-IR pulse in respect to its envelope, called Carrier-Envelope Phase (CEP), is one of the most important parameter in the description of the electric field of such pulses. Hence, good control over its stability is needed in all of the above mentioned scenarios. Passive stabilization methods can be used to generate Mid-IR pulses with intrinsically locked CEP. Indeed, difference frequency mixing of NIR pulses obtained by the

[1] Insulator-metal transitions, superconductivity, change of the magnetic proprieties and many more.

[2] Hight Harmonic Generation just to mention one.

same broadband super-continuum white light generates CEP stable Mid-IR fields. Often this is not enough to maintain the CEP constant over long periods of time, therefore active stabilization methods are also employed.

In this text we present an experimental setup for generating Mid-IR pulses with the above characteristics. After some needed general theory and practical knowledge are given we discuss the possibility of a new time-domain stabilization method based on the well known free space Electro Optic Sampling (EOS) technique. Hence we compare it with the already working frequency-domain approach based on similar processes, which has been demonstrated by Manzoni et al. in their paper[1]. We then prove a proposed method to generate Mid-IR pulses with narrow-band spectra that can be used in particular experiments that call for an higher spectral resolution.

1.2 Sommario

Negli ultimi anni una crescente attenzione è stata posta a sorgenti di impulsi ultracorti nel medio infrarosso (Mid-IR). Per esse è stato dimostrata la possibilità di guidare e sondare una vasta moltitudine di eccitazioni elementari di bassa energia in molecole così come nei solidi. Il controllo di questi processi è particolarmente affascinante per quanto riguarda i materiali a forte correlazione elettronica nei quali, anche piccoli cambiamenti nella struttura cristallografica possono risultare in effetti macroscopici molto rilevanti[3]. Per queste, e molte altre applicazioni[4] la riproducibilità del campo elettrico tra un impulso e l'altro, in fase come in frequenza, è fondamentale. Il processo di generazione di frequenza differenza tra due fasci nel vicino infrarosso provenienti da amplificatori ottici parametrici è stato a lungo utilizzato con successo per generare campi elettrici intensi nel medio infrarosso con durata temporale che si avvicina al limite imposto dalla banda (transform-limited). Lo sfasamento temporale relativo della portante di un impulso Mid-IR rispetto al suo inviluppo, denominato Carrier-Envelope Phase (CEP), è uno dei parametri più importanti nella descrizione del campo elettrico di questi impulsi. Quindi, in tutti gli scenari sopra citati è necessario avere un buon controllo sulla sua stabilità. È possibile utilizzare metodi di stabilizzazione pasiva per generare impulsi Mid-IR con CEP intrinsecamente costante. Infatti, la frequenza differenza generata da due impulsi nel vicino infrarosso, ottenuti a loro volta da uno stesso supercontinuo di "luce bianca", risulta avere CEP stabile. Spesso, però, questo non è sufficiente per mantenere la CEP costante su periodi di tempo lunghi, per questo vengono utilizzati anche metodi di stabilizzazione attiva.

In questo testo presentiamo un setup sperimentale capace di generare impulsi Mid-IR con le caratteristiche appena presentate. Dopo aver dato una dovuta in-

[3] Transizioni metallo-isolante, superconduttività, cambiamenti dello stato magnetico e molti altri.

[4] La generazione di armoniche di ordine elevato, giusto per nominarne una.

farinatura teorica e aver introdotto alcune conoscenze specifiche discutiamo la possibilità di un nuovo metodo di stabilizzazione nel dominio del tempo, basato sulla ben nota tecnica del campionamento Elettro-Ottico (EOS). Quindi lo confrontiamo con il consolidato approccio nel dominio delle frequenze, basato su processi similari, che è stato dimostrato da Manzoni et al. nel loro articolo[1]. Successivamente testiamo un metodo proposto per generare impulsi Mid-IR a banda stretta che possono essere utili in alcuni esperimenti che richiedono una risoluzione spettrale maggiore.

Un primo capitolo è riservato all'introduzione di alcuni concetti fondamentali di teoria degli impulsi. Dapprima si ricava la ben nota equazione di Helmholtz dalle equazioni di Maxwell; essa viene quindi utilizzata per ricavare l'andamento di un generico impulso ideale nell'approssimazione di polarizzazione lineare del mezzo. Facendo uso dell'approssimazione di inviluppo lentamente variabile si ricavano i termini di dispersione nel mezzo, quindi si ricava l'andamento tipico di un impulso gaussiano in un mezzo con dispersione lineare. Vengono introdotti i concetti di chirping del impulso in un mezzo. Segue una descrizione del regime di modelocking nei laser a titanio-zaffiro e si spiega il fenomeno del self phase modulation accennando successivamente all'amplificazione di impulsi chirpata (CPA).

Un altro capitolo è dedicato agli effetti della polarizzazione non lineare nel mezzo sugli impulsi ultracorti. Vengono derivate le equazioni accoppiate che sono responsabili per gli effetti di second'ordine e successivamente sono utilizzate per spiegare i fenomeni di amplificazione ottica parametrica e di generazione di frequenza differenza. Varie approssimazioni sono introdotte e successivamente parzialmente rilassate. È data la descrizione di alcune tecniche per ottenere la condizione di Phase Matching.

Il successivo capitolo si occupa nello specifico di esporre come è fatto, come funziona e a cosa serve il setup sperimentale, occupandosi di spiegare come ogni parte sia fondamentale e perché sono state fatte determinate scelte progettuali rispetto ad altre. Schemi più o meno dettagliati sono presentati per chiarire alcuni aspetti. Si introduce e discute quindi un metodo di stabilizzazione passiva basato sulla generazione di un supercontinuo di luce bianca, da usare come base per l'amplificazione ottica parametrica. Gli spettri degli impulsi nel vicino infrarosso sono mostrati e commentati. Si prosegue quindi con la descrizione del setup di generazione di impulsi nel medio infrarosso, particolare attenzione è riservata alla scelta dello spessore del cristallo di generazione. Vengono quindi presentati degli impulsi coi relativi spettri che dimostrano le caratteristiche di flessibilità e qualità del setup, alcuni dati salienti sono citati.

Nel penultimo capitolo si discute un sistema di misura e rilevazione di impulsi Mid-IR capace di ricostruire l'andamento del campo elettrico in frequenza e fase. Due metodi di stabilizzazione attiva sono presentati, dei quali uno nel dominio della frequenza e uno nel dominio del tempo. Il primo è un metodo già testato[1] e trovato adatto allo scopo. Il secondo invece è sottoposto a test, misure e prove che ne attestano la bontà. Vengono quindi mostrati e comparati i risultati osservando una sostanziale equipollenza delle due tecniche. Infine un ultimo paragrafo è dedicato alla presentazione di un metodo capace di generare impulsi Mid-IR a banda stretta sfruttando il chirping lineare degli impulsi nel vicino infrarosso. Una spiegazione intuitiva del modello è data e successivamente vengono mostrati risultati promettenti che confermano la bontà della tecnica e quindi il suo possibile potenziale.

Nell'ultimo capitolo vengono riassunti i risultati ottenuti e le conclusioni.

Chapter 2

Elements of Ultrafast Optics

2.1 Maxwell and Helmholtz equations

Ultrafast Optics is the branch of optics dealing with the interaction of ultrashort light pulses with matter happening typically on ultrashort timescale. An ultrashort light pulse is a pulse whose time duration is of same timescale as the period of the central carrier wave.

It is common practice to begin every optics' explanation from Maxwell's equations and here we will make no exception to that[1]. In fact from that we will extract the equations that model the ultrashort pulse propagation.

$$\nabla \cdot \mathbf{D} = \rho \tag{2.1}$$

$$\nabla \times \mathbf{E} = -\frac{\partial \mathbf{B}}{\partial t} \tag{2.2}$$

$$\nabla \cdot \mathbf{B} = 0 \tag{2.3}$$

$$\nabla \times \mathbf{B} = \mu_0 \left(\mathbf{J} + \frac{\partial \mathbf{B}}{\partial t} \right) \tag{2.4}$$

where:

[1]Here, and from now on, we will neglect every unuseful explanation on the meanings of the symbols where not strictly needed (E.g., E is the Electric Field, P is the polarization, ...)

$$\mathbf{D} = \epsilon_0 \mathbf{E} + \mathbf{P} \tag{2.5}$$

$$\mathbf{B} = \mu_0 \mathbf{H} + \mathbf{M} \tag{2.6}$$

We can suppose that no free charges nor free currents are present in the material and that it is not magnetized, so that:

$$\rho = 0 \quad \mathbf{J} = 0 \quad \mathbf{M} = 0 \tag{2.7}$$

Now if we apply $\nabla\times$ to (2.2) we obtain:

$$\nabla \times \nabla \times \mathbf{E} = \nabla \times \left(-\frac{\partial \mathbf{B}}{\partial t} \right) = -\frac{\partial}{\partial t} \left(\nabla \times \mathbf{B} \right) = -\frac{\partial}{\partial t} \left(\mu_0 \frac{\partial \mathbf{D}}{\partial t} \right) = -\mu_0 \frac{\partial^2 \mathbf{D}}{\partial t^2} \tag{2.8}$$

in which we also used eq. (2.4) and one of the conditions in (2.7). But since:

$$\nabla \times \nabla \times \mathbf{E} = \nabla \left(\nabla \cdot \mathbf{E} \right) - \nabla^2 \mathbf{E} = -\nabla^2 \mathbf{E} \tag{2.9}$$

hence,

$$\nabla^2 \mathbf{E} = \mu_0 \frac{\partial^2 \mathbf{D}}{\partial t^2} = \mu_0 \frac{\partial^2}{\partial t^2} \left(\epsilon_0 \mathbf{E} + \mathbf{P} \right) = \mu_0 \epsilon_0 \frac{\partial^2 \mathbf{E}}{\partial t^2} + \mu_0 \frac{\partial^2 \mathbf{P}}{\partial t^2} = \frac{1}{c^2} \frac{\partial^2 \mathbf{E}}{\partial t^2} + \mu_0 \frac{\partial^2 \mathbf{P}}{\partial t^2} \tag{2.10}$$

leading to the famous:

$$\nabla^2 \mathbf{E} - \frac{1}{c^2} \frac{\partial^2 \mathbf{E}}{\partial t^2} = \mu_0 \frac{\partial^2 \mathbf{P}}{\partial t^2} \tag{2.11}$$

If we consider a plane-wave like propagation, for which $\mathbf{E}(\mathbf{r}, t)$ is simply E(z,t) we

obtain:

$$\frac{\partial^2 E(z,t)}{\partial z^2} - \frac{1}{c^2}\frac{\partial^2 E(z,t)}{\partial t^2} = \mu_0 \frac{\partial^2 \mathbf{P}}{\partial t^2} \tag{2.12}$$

Which is the equation that represents the propagation of light through a medium (often referred to as Helmholtz equation). If we manage to solve this equation we can obtain the electric field of our pulse in any time and space (given the initial electric field shape).

2.2 Laser Pulse traveling into Matter

The induced dielectric polarization $\mathbf{P}$ can be expanded into:

$$\mathbf{P} = \mathbf{P}_0 + \epsilon_0 \boldsymbol{\chi}^{(1)}\mathbf{E} + \epsilon_0 \boldsymbol{\chi}^{(2)}\mathbf{E}^2 + \epsilon_0 \boldsymbol{\chi}^{3}\mathbf{E}^3 + ... \tag{2.13}$$

Where $\boldsymbol{\chi}^{(i)}$ are, in general, tensors. If we neglect ${\mathbf{P}_0}^2$, we can decompose the $\mathbf{P}$ vector respectively into linear and nonlinear part:

$$\mathbf{P} = \mathbf{P}_L + \mathbf{P}_{NL} \tag{2.14}$$

Where of course:

$$\mathbf{P}_L = \epsilon_0 \boldsymbol{\chi}^{(1)}\mathbf{E} \tag{2.15}$$

$$\mathbf{P}_{NL} = \epsilon_0 \boldsymbol{\chi}^{(2)}\mathbf{E}^2 + \epsilon_0 \boldsymbol{\chi}^{3}\mathbf{E}^3 + ... \tag{2.16}$$

And, as a first approximation[3], assuming that the pulse is not intense enough to

[2]We can do this since then we will take the second derivative in respect to time that will have been anyway zero for this particular term.

[3]In fact we will then relax it, in one of the next sections.

generate nonlinear behaviors, we can neglect $\mathbf{P}_{NL}$ and rewrite the equation (2.12):

$$\frac{\partial^2 E(z,t)}{\partial z^2} - \frac{1}{c^2}\frac{\partial^2 E(z,t)}{\partial t^2} = \mu_0 \frac{\partial^2 \mathbf{P}_L}{\partial t^2} \tag{2.17}$$

Now, for a given electric field pulse shape and a specific $\boldsymbol{\chi}^{(1)}$, we can compute $\mathbf{P}_L$ and solve the eq. (2.17). We can model an ultrashort pulse by multiplying a sinusoid with an envelope function like this:

$$E(z,t) = Re\{\mathcal{A}(z,t)e^{i(\omega_0 t - k_0 z)}\} \tag{2.18}$$

That leads to an electric field pulse shape looking like the one in Figure 2.1[4].

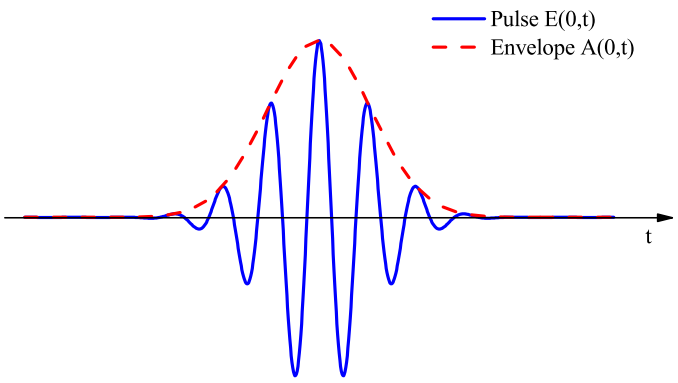

Figure 2.1: Pulse example.

Assuming that the pulse travels through a linear, isotropic and homogeneous material, $\chi^{(1)}$ is a scalar, therefore we can obtain $\mathbf{P}_L$ from E(z,t):

$$\mathbf{P}_L = P_L(z,t) = \epsilon_0 \chi^{(1)} E(z,t) = Re\{\mathcal{P}(z,t)e^{i(\omega_0 t - k_0 z)}\} \tag{2.19}$$

[4]Here $\mathcal{A}(z,t)$ is a Gaussian.

Now we are able to solve the eq. (2.17) with the help of the Fourier transform. We can use a notation such as:

$$\tilde{F}(\omega) = \mathscr{F}\{f(t)\} = \int_{-\infty}^{+\infty} f(t)e^{-i\omega t}dt \tag{2.20}$$

And recalling that:

$$\mathscr{F}\left\{\frac{\partial^n f(t)}{\partial t^n}\right\} = (i\omega)^n \tilde{F}(\omega) \tag{2.21}$$

We obtain:

$$\frac{\partial^2 \tilde{E}}{\partial z^2} + \frac{\omega^2}{c^2}\tilde{E} = -\mu_0 \omega^2 \tilde{P}_L \tag{2.22}$$

with $\tilde{E}$ and $\tilde{P}_L$:

$$\tilde{E}(z,\omega) = \tilde{\mathcal{A}}(z,\omega-\omega_0)e^{-ik_0 z} \tag{2.23}$$

$$\tilde{P}_L(z,\omega) = \tilde{\mathcal{P}}(z,\omega-\omega_0)e^{-ik_0 z} \tag{2.24}$$

where of course:

$$\tilde{\mathcal{A}}(z,\omega-\omega_0) = \int_{-\infty}^{+\infty} \mathcal{A}(z,t)e^{-i(\omega-\omega_0)t}dt \tag{2.25}$$

$$\tilde{\mathcal{P}}(z,\omega-\omega_0) = \int_{-\infty}^{+\infty} \mathcal{P}(z,t)e^{-i(\omega-\omega_0)t}dt \tag{2.26}$$

Then we compute the second derivative of $\tilde{E}$:

$$\frac{\partial^2 \tilde{E}}{\partial z^2} = e^{-ik_0 z}\left(-k_0^2\tilde{\mathcal{A}} - 2ik_0\frac{\partial \tilde{\mathcal{A}}}{\partial z} + \frac{\partial^2 \tilde{\mathcal{A}}}{\partial z^2}\right) \tag{2.27}$$

Under the Slowly Varying Envelope/Amplitude Approximation (SVEA) we can neglect $\partial^2\tilde{A}/\partial z^2$ supposing that:

$$\frac{\partial^2 \tilde{\mathcal{A}}}{\partial z^2} << 2i\,\frac{2\pi}{\lambda_0}\,\frac{\partial \tilde{\mathcal{A}}}{\partial z} \tag{2.28}$$

That is reasonable if we don't have an extreme focusing of the beam. So we end up with eq. (2.22) looking like this:

$$k_0^2\tilde{\mathcal{A}} + 2ik_0\frac{\partial \tilde{\mathcal{A}}}{\partial z} - \frac{\omega^2}{c^2}\tilde{A} = \mu_0\omega^2\tilde{\mathcal{P}} \tag{2.29}$$

The polarization term can be written as:

$$\mu_0\epsilon_0\omega^2\chi^{(1)}\tilde{\mathcal{A}} = \frac{\omega^2}{c^2}\chi^{(1)}\tilde{\mathcal{A}} = \frac{\omega^2}{c^2}\left(n^2-1\right)\tilde{\mathcal{A}} \tag{2.30}$$

And since:

$$k(\omega) = \frac{\omega}{c}n(\omega) \tag{2.31}$$

We get:

$$2ik_0\frac{\partial \tilde{\mathcal{A}}}{\partial z} = [k^2(\omega) - k^2(\omega_0)]\tilde{\mathcal{A}} \tag{2.32}$$

We can manipulate the expression $[k^2(\omega) - k^2(\omega_0)]$, supposing that $k(\omega) \approx k(\omega_0)$, as it follows:

$$[k^2(\omega) - k^2(\omega_0)] = [k(\omega) + k(\omega_0)][k(\omega) - k(\omega_0)] \approx 2k(\omega_0)[k(\omega) - k(\omega_0)] \tag{2.33}$$

That leads to[5]:

$$i\frac{\partial\tilde{\mathcal{A}}}{\partial z} = [k(\omega) - k(\omega_0)]\tilde{\mathcal{A}} \tag{2.34}$$

Now we expand $k(\omega)$ in Taylor series around ω_0:

$$k(\omega) = k(\omega_0) + \left.\frac{dk}{d\omega}\right|_{\omega_0}(\omega-\omega_0) + \frac{1}{2}\left.\frac{d^2k}{d\omega^2}\right|_{\omega_0}(\omega-\omega_0)^2 + \frac{1}{6}\left.\frac{d^3k}{d\omega^3}\right|_{\omega_0}(\omega-\omega_0)^3 + \dots \tag{2.35}$$

And by cutting the expansion we obtain[6]:

$$i\frac{\partial\tilde{\mathcal{A}}}{\partial z}(z,\omega-\omega_0) = \left[k_0^{'}(\omega-\omega_0) + \frac{1}{2}k_0^{''}(\omega-\omega_0)^2 + \frac{1}{6}k_0^{'''}(\omega-\omega_0)^3\right]\tilde{\mathcal{A}}(z,\omega-\omega_0) \tag{2.36}$$

Looking at the definition of group velocity ($v_g = \frac{d\omega}{dk}$), we easily see that $k_0^{'}$ is just:

$$k_0^{'} = \left.\frac{dk}{d\omega}\right|_{\omega_0} = \frac{1}{v_{g_0}} \tag{2.37}$$

Where the group velocity is the velocity at which the envelope of the packet travels through a medium.

We can call $k_0^{''}$ as Group Velocity Dispersion (GVD) around ω_0. In fact since the group velocity itself is, in general, a function of the wave's frequencies, different frequencies will have different group velocity and so there will be a dispersion of them in the pulse.

$$k_0^{''} = \left.\frac{d^2k}{d\omega^2}\right|_{\omega_0} = \text{Group Velocity Dispersion (GVD)} \tag{2.38}$$

[5]Since k_0 stand for k with $\omega = \omega_0$.

[6]Where we denoted $\left.\frac{d^{(i)}k}{d\omega^{(i)}}\right|_{\omega_0}$ as k_0^i

Higher terms correspond, of course, to higher dispersion orders. So we can write:

$$i\frac{\partial\tilde{\mathcal{A}}}{\partial z}(z,\omega-\omega_0)=\left[\frac{1}{v_{g_0}}(\omega-\omega_0)+\frac{\mathrm{GVD}}{2}(\omega-\omega_0)^2+\frac{1}{6}k_0'''(\omega-\omega_0)^3\right]\tilde{\mathcal{A}}(z,\omega-\omega_0) \tag{2.39}$$

We can now use the inverse Fourier Transform to get back to time domain, just remembering the propriety of the inverse Fourier Transform:

$$\mathscr{F}^{-1}\left\{\omega^n\tilde{\mathcal{F}}(\omega)\right\}=(-i)^n\,\frac{d^nf(t)}{dt^n} \tag{2.40}$$

and, therefore:

$$\frac{\partial\mathcal{A}}{\partial z}+\frac{1}{v_{g_0}}\frac{\partial\mathcal{A}}{\partial t}-\frac{i}{2}\,\mathrm{GVD}\,\frac{\partial^2\mathcal{A}}{\partial t^2}+\frac{1}{6}\,k_0'''\,\frac{\partial^3\mathcal{A}}{\partial t^3}=0 \tag{2.41}$$

To simplify even more the equation, so that it can be easily solved, even analytically, we will operate a change of reference frame, from one that is fixed with the medium to one that is moving with the pulse:

$$\begin{cases}\xi=z\\ \tau=t-\dfrac{z}{v_{g_0}}\end{cases} \tag{2.42}$$

This implies that:

$$\begin{cases}\dfrac{\partial}{\partial z}=\dfrac{\partial}{\partial\xi}\dfrac{\partial\xi}{\partial z}+\dfrac{\partial}{\partial\tau}\dfrac{\partial\tau}{\partial z}=\dfrac{\partial}{\partial\xi}-\dfrac{1}{v_{g_0}}\dfrac{\partial}{\partial\tau}\\ \dfrac{\partial}{\partial t}=\dfrac{\partial}{\partial\xi}\dfrac{\partial\xi}{\partial t}+\dfrac{\partial}{\partial\tau}\dfrac{\partial\tau}{\partial t}=\dfrac{\partial}{\partial\tau}\end{cases}^{7} \tag{2.43}$$

So our equation simplifies into:

[7] So in general also $\frac{\partial^n}{\partial t^n}=\frac{\partial^n}{\partial\tau^n}$.

$$\frac{\partial \mathcal{A}}{\partial \xi} - i\frac{\mathrm{GVD}}{2}\frac{\partial^2 \mathcal{A}}{\partial \tau^2} + \frac{1}{6}\, k_0'''\, \frac{\partial^3 \mathcal{A}}{\partial \tau^3} = 0 \tag{2.44}$$

This is the equation we want to solve in the case of purely linear polarization of the medium. In vacuum the solution is trivial. In fact vacuum is a non-dispersive medium so $n(\omega)$ is constant, therefore all $k_0^{(i)}$ are equal to zero except k_0' (but GVD included)[8]. Hence:

$$\frac{\partial \mathcal{A}}{\partial \xi} = 0 \implies \mathcal{A}(\xi, \tau) = const. \tag{2.45}$$

So the pulses travel undisturbed through vacuum. But what does it happen if we add even just the first term in the expansion, that is GVD, so imposing a linear behavior of $n(w)$? We can make use again of the Fourier transform and we get:

$$\frac{\partial \tilde{\mathcal{A}}(\xi, \omega)}{\partial \xi} = -i\frac{\mathrm{GVD}}{2}\omega^2 \tilde{\mathcal{A}}(\xi, \omega) \tag{2.46}$$

And so we can separate the variables and integrate between 0 and a generic L. That result in:

$$\tilde{\mathcal{A}}(L, \omega) = \tilde{\mathcal{A}}(0, \omega)\ \exp\left\{-i\frac{\mathrm{GVD}}{2}\omega^2 L\right\} \tag{2.47}$$

Now if we inverse transform back, we get the final solution:

$$\mathcal{A}(L, t) = \frac{1}{2\pi}\int_{-\infty}^{+\infty} \tilde{\mathcal{A}}(0)\ \exp\left\{-i\frac{\mathrm{GVD}}{2}\omega^2 L\right\} \exp\{i\omega t\} d\omega \tag{2.48}$$

So if one knows $\mathcal{A}(0, t)$, L and GVD then $\mathcal{A}(L, t)$ can be compute. But this is

[8]This because as we already said that $k_0^i = \frac{d^{(i)}k}{d\omega^{(i)}}\Big|_{\omega_0} = \frac{d^{(i)}}{d\omega^{(i)}}(\frac{\omega n(\omega)}{c})\Big|_{\omega_0} = \frac{\omega_0}{c}\frac{d^{(i)}n(\omega_0)}{d\omega^{(i)}}$.

possible, in general, only numerically, in which case we could also add higher terms like k_0''' and so on. There is anyway an analytical solution, that implies, of course[9], a Gaussian envelope. Let's take so a Gaussian pulse:

$$\mathcal{A}(0,t) = \mathcal{A}_0 \exp\left(-\frac{t^2}{2\tau_p^2}\right) \tag{2.49}$$

Where τ_p is proportional to the Full Width at Half Maximum (FWHM) of the pulse, so it's linked directly to the time duration of the pulse. As we know the Fourier transform of a Gaussian such as this one is:

$$\mathscr{F}\left\{\mathcal{A}_0 \exp\left(-\frac{t^2}{2\tau_p^2}\right)\right\} = \mathcal{A}_0\sqrt{2\pi}\,\tau_p \exp\left(-\frac{\omega^2}{2}\tau_p^2\right) = \tilde{\mathcal{A}}(0,\omega) \tag{2.50}$$

That is still a Gaussian. Moreover the time-duration and the frequency bandwidth of the pulse are inversely proportional. This assertion is true, of course, for every envelope shape and it's due to the time-frequency dichotomy. Now, if we put this into eq. (2.47) and renaming the product of GVD$\cdot L$ as Group Delay Dispersion (GDD) or D_2, we get:

$$\tilde{\mathcal{A}}(L,\omega) = \mathcal{A}_0\sqrt{2\pi}\,\tau_p\, \exp\left(-\frac{\omega^2\tau_p^2}{2}\left[1 + i\frac{D_2}{\tau_p^2}\right]\right) \tag{2.51}$$

By inverse Fourier transforming this back and separate the real and imaginary part of the exponential we obtain the final solution that is:

$$\mathcal{A}(L,t) = \frac{\mathcal{A}_0\tau_p}{\sqrt{\tau_p^2 + iD_2}}\, \exp\left(-\frac{t^2}{2\tau_{out}^2}\right)\, \exp\Big(i\varphi(t)\Big) \tag{2.52}$$

Where:

[9] Bearing in mind that Gaussians are eigenvalues of the Fourier Transform.

$$\begin{cases} \tau_{out}^2 = \tau_p^2 \left[1 + \left(\dfrac{\text{GVD} \cdot L}{\tau_p^2}\right)^2\right] = \tau_p^2 \left[1 + \left(\dfrac{L}{L_D}\right)^2\right] \\ \varphi(t) = \dfrac{D_2\, t^2}{2\left(\tau_p^4 + {D_2}^2\right)} \end{cases} \qquad \text{with } L_D = \frac{\tau_p^2}{\text{GVD}} \tag{2.53}$$

The first term in eq. (2.53) is the time-duration of a Gaussian pulse propagated for a length L into a dispersive medium (so with a non-zero GVD). It is a parabolic equation so there is a minimum of the time duration and then the pulse start to stretch and becomes longer and longer. To have an even easier understanding of the phenomena we can also rewrite it as:

$$\begin{cases} if \quad L << L_D \implies \tau_{out} \simeq \tau_p \\ if \quad L >> L_D \implies \tau_{out} \simeq \tau_p \, \dfrac{L}{L_D} \end{cases} \tag{2.54}$$

And this can be also demonstrated to be true for every envelope shape under some sort of approximation, not only for a Gaussian one. So, first of all, a pulse traveling through a medium always comes out stretched, and the shorter it is in time before the more it will be stretched after. Indeed, a short pulse will have a small L_D so it will tend to spread out "quicker" than a longer pulse.
If we look at the phase in eq. (2.53) and considering that our envelope $\mathcal{A}(L,t)$ is multiplied by $e^{i(\omega_0 t - k_0 z)}$ (look at eq. (4.1)) we end up with an instantaneous frequency:

$$\omega_i(t) = \frac{d}{dt}\left[\omega_0 t + \varphi(t)\right] = \omega_0 + \frac{D_2 t}{\left(\tau_p^4 {D_2}^2\right)} \tag{2.55}$$

That means that the frequencies of the pulse become spread along the pulse, so they do not come all together anymore. This phenomena is called Chirp[10]. We

[10]The name is a reference to chirping in analogy to the sound made by some birds.

have two typical example of chirped pulse in Figure 2.2 and in Figure 2.3, corresponding of different sign of GVD (that determines the sign D_2).

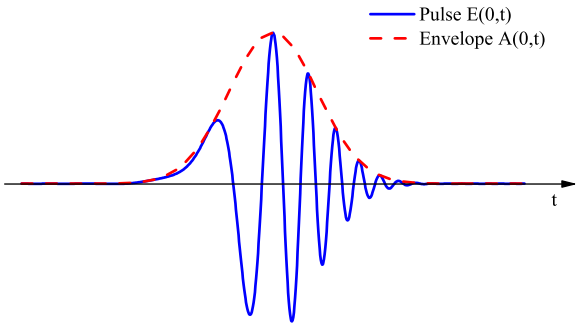

Figure 2.2: Up-Chirped pulse, often referred to as Positive Chirped or Blue-Chirped Pulse. In fact GVD (D_2) is positive and so higher frequencies ("Blue") come later in time in respect to lowers ("Red").

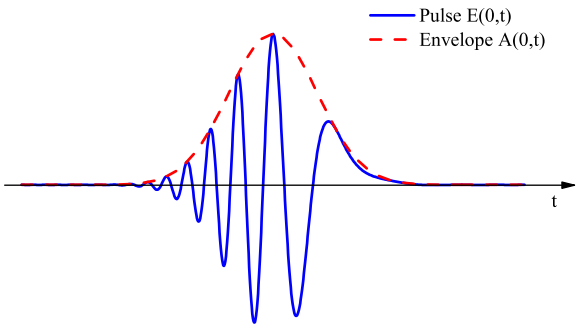

Figure 2.3: Down-Chirped pulse, often referred to as Negative Chirped or Red-Chirped Pulse. Is the opposite of the Up-Chirped.

Normally most of the materials happen to have GVD positive for a quite broad range of frequencies, but there are cases in which the opposite is true[11]. The chirp produced by a non-zero GVD it's called linear since the dispersion of the

[11]E.g fused silica glass has a negative GVD in a window around 1.5 μm

instantaneous frequencies along the pulse is linear as we can see in eq. (2.55). Considering higher terms in eq. (2.35), that implies considering a more than quadratic behavior of k in respect to ω, would have meant obtaining higher than linear dependence of the instantaneous frequency (ω_i) in respect to time. So for example if we kept the k_0''' term, that means considering a cubic behavior of k, we would obtain a quadratic dependence of ω_i.

The shortest pulse is achieved when the pulse is un-chirped, so that all the terms higher than $k_0{}'$ are zero and the time duration of the pulse is limited just by the spectral bandwidth due to the Fourier transform. Such pulses are called Transform Limited (TL). To obtain a TL pulse one have to avoid the chirping of the pulse by maintaining low values for the dispersion coefficients for the chosen wavelength. But this is not always possible, so, in such cases, one can design an optical system that compensate for the chirp induced. This system are called compressors and their dispersion coefficients' values are chosen to be the opposite of the ones of the system that has to be compressed.

One may want to do the opposite, so add a chirp to the pulse to elongate it. The systems responsible for this action are called stretchers, and they usually induce a well-chosen dispersion to the pulse so that it can travel through the optical system avoiding any unwanted behavior[12] and then, if needed, it can be easily compressed back to the initial temporal length.

2.3 Chirped Pulse Amplified Mode-locked Laser

Before going deeper into the field of ultrashort pulses propagating in a medium let's introduce briefly how an ultrashort pulse can be obtained.

[12]E.g. high order dispersion that are usually difficult to compensate for and also non-linear effect that will be discussed in one of the following section

As we already mentioned an ultrashort pulse has a time duration comparable with the period of the central wavelength of the packet. So for example a pulse in the visible light range could have time duration down to few femtoseconds.

The method more widely used to produce such pulses is using a Modelocked Laser (ML) as a source. A laser is, in principle, just a gain medium in a cavity optically or electrically pumped. In Continuous Wave (CW) regime the laser oscillates on a single or only few longitudinal modes which fit the boundary conditions imposed by the cavity. But in principle the possible lasing modes are more, in fact there are multiple modes for which the unsaturated gain is bigger than one. So a laser operating in multi-mode regime will, in general, produce an output that is not constant in time (since it is not a single wave). Its time distribution depends on the phase relations between the active modes of the cavity.

If the phases' relations are chosen properly the output can be a train of pulses. As always the time duration of each pulse will be related through the Fourier Transform to the bandwidth available, so one of the basic requirements for such laser is to have a broad gain bandwidth and therefore a lots of active modes.

Let's now suppose to have a laser running into multi-mode regime with an active gain linewidth $\Delta\omega_g$ and $2N-1$ active mode separated by $\Delta\omega = 2\pi\frac{c}{L}$, imposed by the cavity. With the usual plane wave approximation we can write the electric field in the cavity as:

$$E(t) = \sum_n A_n e^{i\phi_n} e^{i\omega_n\left(t-\frac{z}{c}\right)} + c.c. \tag{2.56}$$

Where $A_n e^{i\phi_n}$ is the complex amplitude of the nth mode. But if ω_0 is the central wavelength, we can write that $\omega_n = \omega_0 + \Delta\omega n$, and if we change frame of reference

we get:

$$E(t) = \sum_n A_n e^{i\phi_n} e^{i\omega_0 t + i\Delta\omega n t} + c.c. \tag{2.57}$$

In which we can distinguish a slowly varying term that we can call $A(t) = \sum_n A_n e^{i\phi_n} e^{+i\Delta\omega n t}$ and a higher frequency term $e^{i\omega_0 t}$. So $E(t)$ is almost monochromatic, and therefore we can write the intensity as:

$$I(t) \propto |A(t)|^2 = \left| \sum_n A_n e^{i(\phi_n + \Delta\omega n t)} \right|^2 \tag{2.58}$$

If the phases ϕ_n of the modes are uncorrelated one between the other the $I(t)$ resulting will be an intensity with apparently random spikes similar to the one in Figure 2.4.

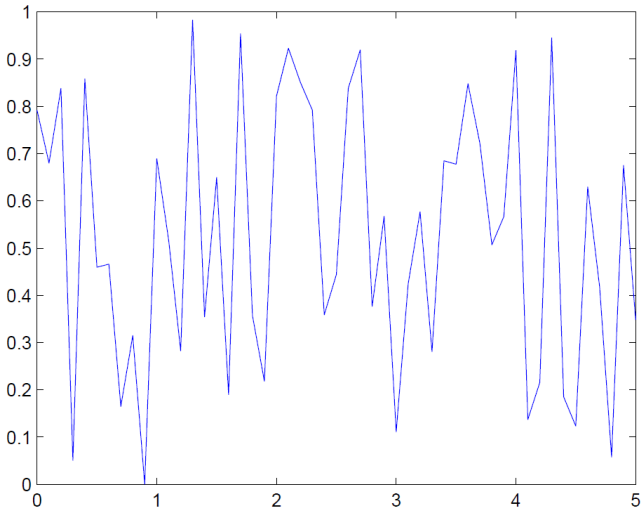

Figure 2.4: Normalized $I(t)$ for a multi-mode laser in free-running regime. From [2].

Such behavior is called free-running mode, and, even if it can be difficult to guess at first glance, is periodic with period $T_R = \frac{2\pi}{\Delta\omega} = \frac{L}{c}$. Moreover every spike has a

time-duration inversely proportional to the total bandwidth of all the modes.

If we impose instead a precise relation between the mode we obtain the mode-lock regime. In fact let's suppose to "lock" the phases in such manner that $\phi_{n+1} - \phi_n = \phi = constant$, or, in other words, $\phi_n = n\phi$, we can write:

$$A(t) = \sum_n A_n e^{in\Delta\omega t + in\phi} = \sum_n A_n e^{in\Delta\omega t'} \tag{2.59}$$

Where $t' = t + \frac{\phi}{\Delta\omega}$. This is a Fourier series, and, in particular, if we suppose that all modes have the same amplitude A_0 this becomes a geometric series with common ratio $\alpha = e^{i\Delta\omega t'}$. The partial sum of such series over $2N-1$ modes between $-N$ and N can be written as follows:

$$A(t) = A_0 \frac{sin\Big(\frac{\Delta\omega t'(2N+1)}{2}\Big)}{sin\big(\frac{\Delta\omega t'}{2}\big)} \tag{2.60}$$

Therefore:

$$I(t) = A_0^2 \frac{sin^2\Big(\frac{\Delta\omega t'(2N+1)}{2}\Big)}{sin^2\big(\frac{\Delta\omega t'}{2}\big)} \tag{2.61}$$

That is graphically represented in Figure 2.5.

This is still a periodic function with the same period $T_R = \frac{2\pi}{\Delta\omega} = \frac{L}{c}$ as before. Anyway here we can notice that there is only one huge pulse every period, and, since the period corresponds to the time needed for the light to travel into the cavity, we can deduce that there is only one pulse at a time inside the cavity. The time duration of this pulse can be retrieved from eq. (2.61):

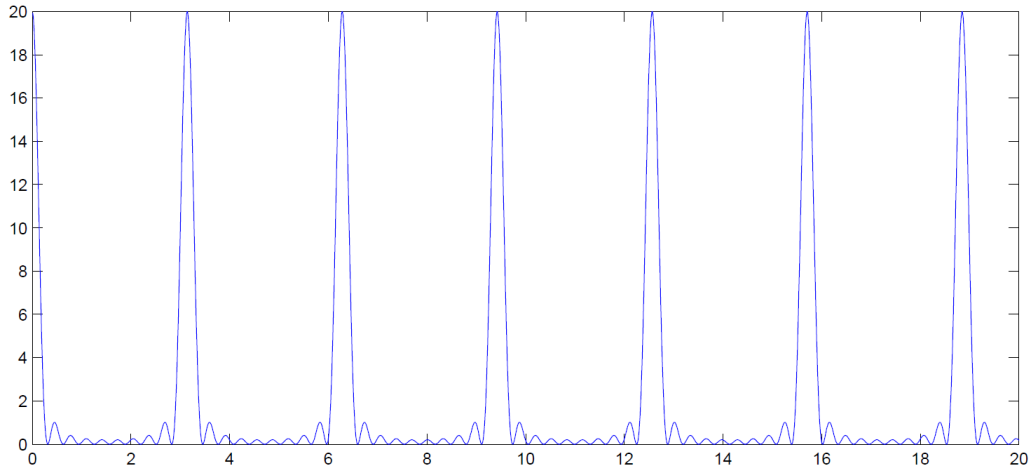

Figure 2.5: Typical $I(t)$ for a multi-mode laser in Mode-lock regime. From [2].

$$\Delta\tau_p \approx \frac{2\pi}{(2N+1)\,\Delta\omega} = \frac{1}{\Delta\nu_{osc}} \tag{2.62}$$

Where we denoted as $\Delta\nu_{osc}$ the total bandwidth of all modes. So the more active modes there are, the more bandwidth can be used, the shorter the pulses can be generated. If we considered the more realistic case in which not all the modes had the same amplitude still we would obtain similar results[13]. We would like to stress here that the relation cited between time duration and available bandwidth is totally equal to the one imposed by the Fourier Transform[14]. Not only, in fact if we assume a more than linear dependence of the phase difference between the modes, we obtain a longer pulse in time, as you would expect from the results of the previous section. This is reasonable if one observe that the mode-locked laser spectrum is the discrete equivalent of the spectrum of a single pulse, and so the general description and comments of the previous sections still hold here.

[13]For example imposing an exponential distribution of the amplitude $A_n = A_0 e^{-|\omega|}$ we obtain a train of exponential shaped pulses with similar characteristics as the one we obtained here.

[14]In fact if we performed a more meticulous calculation we would obtain the Transform Limit pulse relation for that particular amplitude shape.

Summarizing, we have to create a precise relation between the phases of a large number of active modes in a laser to obtain a train of short pulses. First of all let's choose an active medium with a large gain curve width, since as we just said the bigger the available bandwidth the shorter the pulses. In recent year one stood out among all of the others: Ti:Sapphire. The medium is obtained by slightly[15] doping a Sapphire crystal (Al_2O_3) with Titanium Oxide (Ti_2O_3). The Ti^{3+} ion substitutes for the Al^{3+} ion but since the ionic radius of the first is 26% larger than the second's it induces a strong distortion of the local environment. This is the cause of the well know Stark and Jahn-Teller Effect, so the absorption and emission spectra are well separated and broad[16]. So the Sapphire assure good transparency, good thermal conduction and great hardness, that are essential for a stable and durable medium, the Ti doping ion, on the other hand, assures a large vibrational emission spectrum well separated in respect to the absorption one.

The emission spectra of such medium, so, extends between 650 nm up to 1100 nm, with the pick at roughly 800 nm. Instead the absorption is centered around 500 nm with a total bandwidth of almost 200 nm. Hence it is typically optically pumped by frequency-doubled Nd:YAG solid state laser in collinear way[17]. The number of possible active modes for an emission spectra such wide can reach up to tens of thousands, and moreover with all that bandwidth, in principle, one can obtain transform-limited pulses with duration down to few femtoseconds[18].

To obtain the locking of the mode various methods can be exploited. It is possi-

[15] Up to few percent.

[16] Indeed, the absorption happens between the T_g state and a E_g state that are shifted due to the Stark effect. The emission is vibronic, so phonon assisted, and happens between levels shifted due to the Jahn-Teller Effect that is the consequence of the environment stress on the Ti^{3+} excited ion.

[17] It can be pumped by various other lasers such as Ar ion laser (514 nm) or other Nd based solid state lasers.

[18] Nowadays 10 fs pulses is daily routine, and even 3 or 5 fs laser are commercially available.

ble externally modulate the losses or the gain inside the cavity to favor the pulse mode. This kind of technique is called active mode-locking. On the contrary passive methods consist in the insertion of a nonlinear medium inside the cavity that enhance stronger intensities. One of the most interesting technique out of these is the so called Self-Locking of the modes. As we already saw, inside the cavity, during the free-running regime, intensity spikes are normally present. Those are caused by an instantaneous random lock of the phases of some modes that therefore produce a constructive interference. If we suppose to impose a condition that promote the enhancement of higher intensities in respect to the lower's those spikes can grow higher and higher. This will eventually correspond to the locking of the modes.

The presence of a $\chi^{(3)}$ tensor different than zero in a material implies that the refractive index is proportional with the intensity of the light that travels in that material[19]. So we can write $n = n_0 + n_2 I$. This implies that, for n_2 positive[20], the more intense is the Field the bigger the index of refraction it will see. Every pulse usually have an intensity profile that is not constant over the all space, if we assume a Gaussian shaped pulse we can easily write then $I(r)$. When such pulse travels into a material with positive n_2 the effect is the same of a pulse traveling into a material with homogeneous index of refraction, but with Gaussian shape proportional to $I(r)$. Such material is a Gaussian lens. This is why this effect is called Kerr Lens effect or Self-Focusing. During the propagation of a pulse through a thick material this process is enhanced along the path because focusing of the beam increases the focal power of the dynamical lens. This increase of the focusing stops when the diameter of the beam is small enough so that the linear diffraction is large enough to balance the Kerr effect.

[19]Indeed if $P = \epsilon_0 \chi^{(1)} E + \epsilon_0 \chi^{(3)} E^3$ then $\epsilon_r = \chi^{(1)} + \chi^{(3)} E^2$ but since $n = \sqrt{\epsilon_r}$ and $E^2 \propto I$ so $n \approx n_0 + n_2 I$ with $n_2 \propto \chi^{(3)}$.

[20]That is what happens in the majority of the cases.

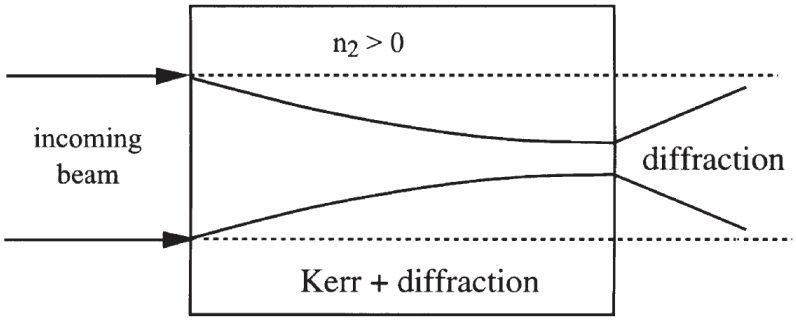

Figure 2.6: Self-focusing of a laser beam crossing a medium with positive n_2. From [3].

The Ti:Sapphire medium has a $\chi^{(3)}$ large enough to produce such phenomenon. It's easy to understand that this is already a method that promotes the establishment of high intensity pulses inside the cavity, since the higher maxima will be more focused and so less sensitive to natural losses of the cavity in respect to weaker intensities that occupy a large volume(Figure 2.7). To enhance even more the losses for unfocused light one can insert a slit or a pinhole on the path of the beam.

This is in principle enough to promote the self mode-locked regime in respect to the continuous wave regime. In reality some big fluctuation in the intensities are needed to kick the positive feedback loop of the Kerr-Lens effect. This is usually obtained by some sort of perturbation of the system[21]. Since the high power induce at least a first order dispersion in such systems it is always needed some sort of compression optics[22].

This system can then produce a stable train of ultrashort pulse with good op-

[21]It can be a real kick, in really basics systems, as well as some vibration produced by a speaker or a rotation of a prism inside the cavity, etc...

[22]It can be a prism pair or some chirp-mirror or others.

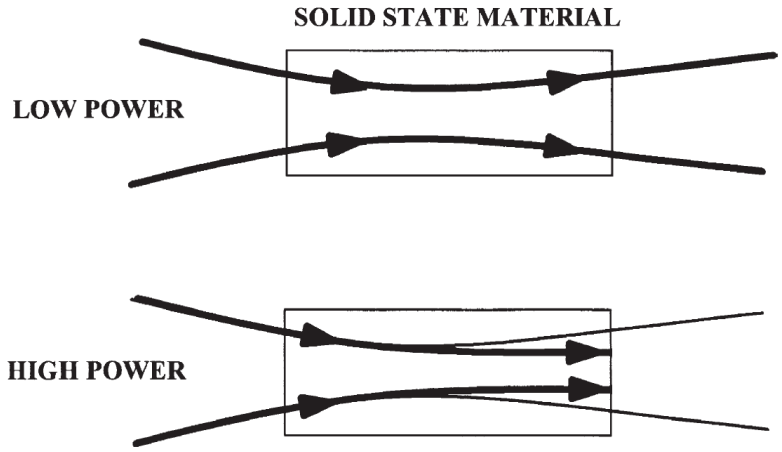

Figure 2.7: Illustration of the self-focusing effect by the optical Kerr effect on the beam waist of a laser beam at high and low intensity. From [3].

tical features. What is difficult to obtain, actually, is really high power. In fact, as we know, the peak power of each pulse is inversely related to its time duration. Ultrashort pulse generated in mode-locked laser can therefore have quite high peak power. If the peak power of an ultrashort pulse is too high all sort of nonlinearities comes up when traveling into a medium. These nonlinearities can cause from a simple stretching of the pulse to a damage of the gain material. To overcome such problem the Chirped Pulse Amplification technique was developed. The idea is quite simple, first of all we divide the system into two simpler systems responsible each for one specific task. The first system, that is an actual mode-locked laser as we just described, is the one that create a stable train of pulse, and it's called Oscillator. This system is tuned and engineered to obtain the best quality and reliability of the pulse duration, shape, repetition rate and stability, but with quite low power. The second stage main task is instead to produce high output power, and this is why it is called Amplifier.

To avoid the already mentioned problems, the trick of the Amplifier is that the pulse is stretched in an optical system that is engineered to induce a chirp in a

well known and controlled manner, then the pulse travels into an active medium that amplifies it, and after that the pulse is compressed back to the previous time duration, obtaining a huge pulse power (Figure 2.8).

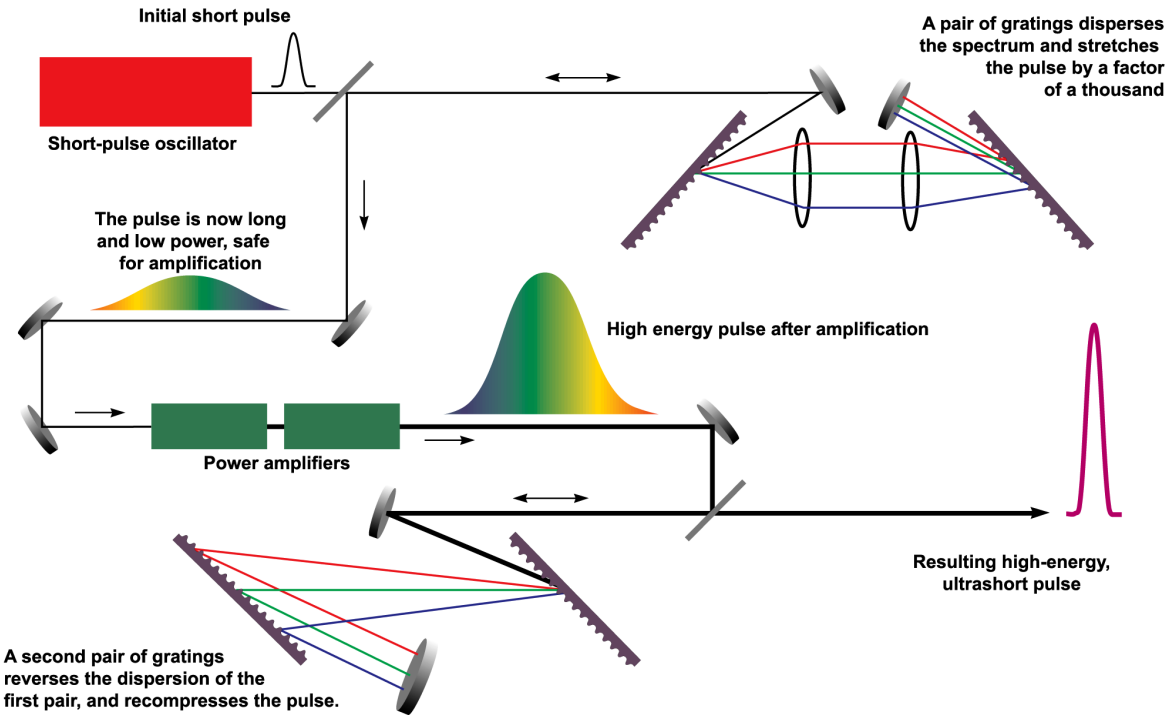

Figure 2.8: Diagrammatic scheme of chirped pulse amplification from [4].

Chapter 3

Nonlinear Polarization

3.1 Coupled Equations

When the superposition principle can be applied to electromagnetic waves or when the proprieties of matter do not depend on the intensity of light, one speaks of linear optics. This is what usually occurs with low-intensity sources. Those sources can be characterized by a set of parameters such as the index of refraction, the absorption and reflection coefficients and the orientation of the medium with respect to the polarization of the light. With the current laser pulsed technology, peak power well beyond the linear regime can be generated. In this large intensity regime the optical parameters become functions of the intensity of the impinging light. The distinction between linear and non-linear regime is usually defined looking at the dependence of the polarization of the material in respect to the Electric Field of the incident light. In the previous chapter we already wrote the polynomial expansion of the polarization of a medium in the eq. (2.13),(2.14),(2.15). In that case we ignored the non linear polarization, if we instead keep it one can write:

$$\frac{\partial^2 E(z,t)}{\partial z^2} - \frac{1}{c^2}\frac{\partial^2 E(z,t)}{\partial t^2} = \mu_0 \frac{\partial^2 P_L}{\partial t^2} + \mu_0 \frac{\partial^2 P_{NL}}{\partial t^2} \tag{3.1}$$

If we assume again a pulse electric field shaped in this way:

$$E(z,t) = Re\{\mathcal{A}(z,t)e^{i(\omega_0 t - k_0 z)}\} \tag{3.2}$$

We can write P_{NL} as:

$$P_{NL}(z,t) = Re\{\mathcal{P}_{NL}(z,t)e^{i(\omega_0 t - k_p z)}\} \tag{3.3}$$

Since the polarization travels at a different speed than the electric field. The second derivative of the polarization is:

$$\frac{\partial^2 P_{NL}}{\partial t^2} = \left[\frac{\partial^2 \mathcal{P}_{NL}}{\partial t^2} + 2i\omega_0 \frac{\partial \mathcal{P}_{NL}}{\partial t} - \omega_0^2 \mathcal{P}_{NL}\right] e^{i(\omega_0 t - k_p z)} \tag{3.4}$$

Under the usual SVEA approximation we can neglect the first two terms in the brackets so that the eq. (3.1) becomes:

$$\frac{\partial^2 E(z,t)}{\partial z^2} - \frac{1}{c^2}\frac{\partial^2 E(z,t)}{\partial t^2} = \mu_0 \frac{\partial^2 P_L}{\partial t^2} - \mu_0\, \omega_0^2\, \mathcal{P}_{NL}\, e^{i(\omega_0 t - k_p z)} \tag{3.5}$$

So following the same steps as before we obtain[1]:

$$\frac{\partial \mathcal{A}}{\partial z} + \frac{1}{v_{g_0}}\frac{\partial \mathcal{A}}{\partial t} - \frac{i}{2}\,\mathrm{GVD}\,\frac{\partial^2 \mathcal{A}}{\partial t^2} = -i\,\frac{\mu_0 \omega_0 c}{2n_0}\,\mathcal{P}_{NL}\, e^{-i\Delta k z} \tag{3.6}$$

Where $\Delta k = k_p - k_0$. We shall now recall:

$$P = \epsilon_0 \left[\chi^{(1)}E + \chi^{(2)}E^2 + \chi^{(3)}E^3 + ...\right] \tag{3.7}$$

[1]For simplicity, here, we neglected the third-order term $\frac{1}{6}\, k_0'''\, \frac{\partial^3 \mathcal{A}}{\partial t^3}$ and all the highers.

When present[2], the most important term is the χ^2, since it gives the strongest non linear response. So let's focus on the second order phenomena. In the most general case we have to write:

$$E(t) = \frac{1}{2}\left[E_1 e^{i(\omega_1 t - k_1 z)} + E_2 e^{i(\omega_2 t - k_2 z)} + c.c.\right] \tag{3.8}$$

So P_{NL} will be:

$$\begin{aligned} P_{NL} = \epsilon_0 \chi^{(2)} E(t)^2 = \\ = \frac{\epsilon_0 \chi^{(2)}}{4}\Big\{ & E_1{}^2 e^{2i(\omega_1 t - k_1 z)} + E_1^{*2} e^{-2i(\omega_1 t - k_1 z)} + \\ & E_2{}^2 e^{2i(\omega_2 t - k_2 z)} + E_2^{*2} e^{-2i(\omega_2 t - k_2 z)} + \\ & 2E_1 E_2 e^{i[(\omega_1+\omega_2)t - (k_1 - k_2)z]} + c.c. + \\ & 2E_2 E_1^* e^{i[(\omega_2 - \omega_1)t - (k_2 - k_1)z]} + c.c. + \\ & E_1 E_1^* + E_2 E_2^* \Big\} \end{aligned} \tag{3.9}$$

But since the polarization of the medium implies an electric field, we can assume that in principle all these terms will be generated in a nonlinear medium. In reality the fundamental requirement for any of these phenomena to be at least appreciable is the phase-matching condition($\Delta k = 0$). In fact only when this happens we have a constructive interference between the polarization and the input-wave and so an effective process. We can sketch these phenomena as it is shown in Figure 3.1.

One should notice that all the terms present in eq. 3.9 correspond to some terms in the sketched Figure 3.1. It can be useful to picture this phenomena in corpuscular terms (Figure 3.2 to 3.5).

[2]The even terms do not exist in every material, since only non-centrosymmetric crystals allow them, whereas the odd terms are always present.

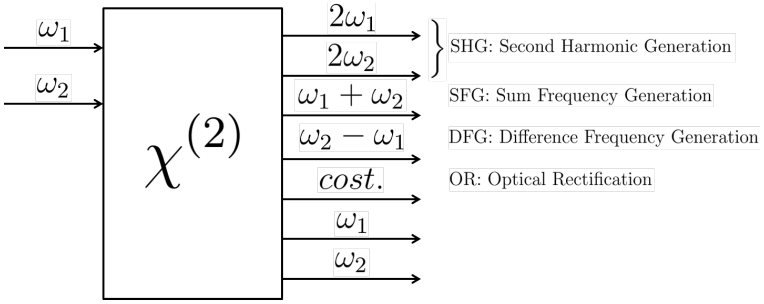

Figure 3.1: Sketched effects of the second-order susceptibility.

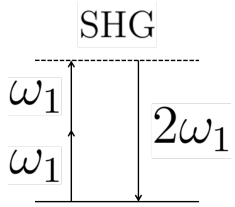

Figure 3.2: Second Harmonic Generation

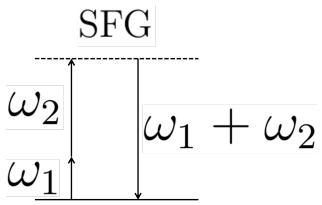

Figure 3.3: Sum Frequency Generation

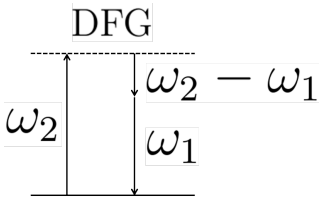

Figure 3.4: Difference Frequency Generation

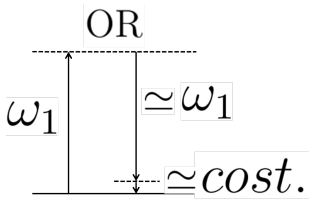

Figure 3.5: Optical Rectification

In the DFG process if one of the beam is stronger than the other, for example $E_{\omega_1} >> E_{\omega_2}$, it can be used to amplify the less intense beam. For this reason this process is called Optical Parametric Amplification (OPA). In this case the strong beam is called pump, the weak one is called signal and the difference beam is called idler. Such process is sketched in Figure 3.6.

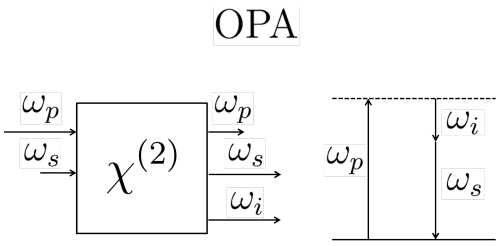

Figure 3.6: Optical Parametric Amplification

Since this is, de facto, a DFG process it follows that $\omega_i = \omega_p - \omega_s$. It is important to notice that here the transitions occur between virtual levels (life-time zero) so there are no selection rules involved. This means that the amplification bandwidth available is very large and so compatible with short pulses.

If we suppose to have three input beams ω_1,ω_2 and $\omega_3 = \omega_1 + \omega_2$, we can write the non-linear polarization at each frequency using the eq. 3.9.

$$P_{NL}^{\omega_1}(z,t) = \tfrac{1}{4}\,\epsilon_0\chi^{(2)}\,2\,\mathcal{A}_3\mathcal{A}_2^*\,e^{i[(\omega_3-\omega_2)t-(k_3-k_2)z]} + c.c. \tag{3.10}$$

$$P_{NL}^{\omega_2}(z,t) = \tfrac{1}{4}\,\epsilon_0\chi^{(2)}\,2\,\mathcal{A}_3\mathcal{A}_1^*\,e^{i[(\omega_3-\omega_1)t-(k_3-k_1)z]} + c.c. \tag{3.11}$$

$$P_{NL}^{\omega_3}(z,t) = \tfrac{1}{4}\,\epsilon_0\chi^{(2)}\,2\,\mathcal{A}_1\mathcal{A}_2\,e^{i[(\omega_1+\omega_2)t-(k_1+k_2)z]} + c.c. \tag{3.12}$$

And hence:

$$\begin{cases} \frac{\partial\mathcal{A}_1}{\partial z} + \frac{1}{v_{g_1}}\frac{\partial\mathcal{A}_1}{\partial t} - \frac{i}{2}\mathrm{GVD}_1\frac{\partial^2\mathcal{A}_1}{\partial t^2} = -i\frac{\mu_0\omega_1 c}{4n_1}\,\epsilon_0\chi^{(2)}\,\mathcal{A}_2^*\mathcal{A}_3\,e^{-i(k_3-k_2-k_1)z} \\ \frac{\partial\mathcal{A}_2}{\partial z} + \frac{1}{v_{g_2}}\frac{\partial\mathcal{A}_2}{\partial t} - \frac{i}{2}\mathrm{GVD}_2\frac{\partial^2\mathcal{A}_2}{\partial t^2} = -i\frac{\mu_0\omega_2 c}{4n_2}\,\epsilon_0\chi^{(2)}\,\mathcal{A}_1^*\mathcal{A}_3\,e^{-i(k_3-k_1-k_2)z} \\ \frac{\partial\mathcal{A}_3}{\partial z} + \frac{1}{v_{g_3}}\frac{\partial\mathcal{A}_3}{\partial t} - \frac{i}{2}\mathrm{GVD}_3\frac{\partial^2\mathcal{A}_3}{\partial t^2} = -i\frac{\mu_0\omega_3 c}{4n_3}\,\epsilon_0\chi^{(2)}\,\mathcal{A}_1\mathcal{A}_2\,e^{-i(k_1+k_2-k_3)z} \end{cases} \tag{3.13}$$

This are coupled equations due to the nonlinearity. If the system was linear we would get the same result as we obtained before, so the usual parabolic equation with the pulses running away one in respect to the other due to the different group velocity and each spreading out due to the second order dispersion (GVD). The leading term in such situation is the group velocity mismatch, so we will neglect the GVD. For the sake of simplicity we can call $d_{\text{eff}} = \chi^{(2)}/2$, $b_i = \omega_i d_{\text{eff}}/2nc$ and $\Delta k = k_3 - k_2 - k_1$. So the system becomes:

$$\begin{cases} \frac{\partial\mathcal{A}_1}{\partial z} + \frac{1}{v_{g_1}}\frac{\partial\mathcal{A}_1}{\partial t} = -ib_1\mathcal{A}_2^*\mathcal{A}_3\,e^{-i\Delta kz} \\ \frac{\partial\mathcal{A}_2}{\partial z} + \frac{1}{v_{g_2}}\frac{\partial\mathcal{A}_2}{\partial t} = -ib_2\mathcal{A}_1^*\mathcal{A}_3\,e^{-i\Delta kz} \\ \frac{\partial\mathcal{A}_3}{\partial z} + \frac{1}{v_{g_3}}\frac{\partial\mathcal{A}_3}{\partial t} = -ib_3\mathcal{A}_1\mathcal{A}_2\,e^{i\Delta kz} \end{cases} \tag{3.14}$$

This is the general form of the coupled equation that govern the second order non linear processes.

3.2 Optical Parametric Amplifier

If we suppose to be dealing with an Optical Parametric Amplifier the pump will be ω_3, the signal is then ω_2 and ω_1 is the idler[3]. So let's suppose to change reference frame according to the pump pulse. The beams will have, in general, different speed in the medium, so one can introduce the Group Velocity Mismatch (GVM) term. We can define it as $\delta_{13} = \frac{1}{v_{g_1}} - \frac{1}{v_{g_3}}$ for the idler in respect to the pump and δ_{23} accordingly for the signal in respect to the pump.

$$\begin{cases} \frac{\partial \mathcal{A}_1}{\partial z} + \delta_{13}\frac{\partial \mathcal{A}_1}{\partial t} = -ib_1\mathcal{A}_2^*\mathcal{A}_3\, e^{-i\Delta kz} \\ \\ \frac{\partial \mathcal{A}_2}{\partial z} + \delta_{23}\frac{\partial \mathcal{A}_2}{\partial t} = -ib_2\mathcal{A}_1^*\mathcal{A}_3\, e^{-i\Delta kz} \\ \\ \frac{\partial \mathcal{A}_3}{\partial z} = -ib_3\mathcal{A}_1\mathcal{A}_2\, e^{i\Delta kz} \\ \end{cases} \tag{3.15}$$

To have a really simple and basic model let's proceed with three approximations. To avoid bothering with time derivative we can assume a very long pulse (at the limit, a monochromatic wave). Then we can suppose that we have fulfilled the Phase Matching (PM) condition so $\Delta k = 0$. In general, since we want to amplify it, $\mathcal{A}_2 << \mathcal{A}_3$, we can therefore also assume that the intensity of the pump pulse $\mathcal{A}_3$ is constant in space. This is called undepleted pump approximation and enables us to write:

$$\begin{cases} \frac{\partial \mathcal{A}_1}{\partial z} = -ib_1\mathcal{A}_2^*\mathcal{A}_{30} \\ \\ \frac{\partial \mathcal{A}_2}{\partial z} = -ib_2\mathcal{A}_1^*\mathcal{A}_{30} \\ \\ \mathcal{A}_3(z) \simeq \mathcal{A}_{30} \\ \end{cases} \tag{3.16}$$

[3]It is common practice to call signal the higher frequency beam in respect to the other output beam that is called idler.

These equations are now easily solvable. If we define $\Gamma = b_1 b_2 |\mathcal{A}_{30}|^2$, and then integrate between 0 and z the first two equations, imposing that $\Gamma z >> 1$, we obtain[4]:

$$\begin{cases} I_1(z) = \frac{I_{10}}{4} e^{2\Gamma z} \\ \\ I_2(z) = \frac{I_{20}}{4} e^{2\Gamma z} \\ \\ I_3(z) \simeq I_{30} \end{cases} \tag{3.17}$$

Where, of course, $I = \frac{1}{2}\epsilon_0 nc|\mathcal{A}|^2$ and $I_1(z) = \frac{\omega_1}{\omega_2} I_2(z)$. So every time one pump photon is annihilated, two photon are created, one idler photon and one signal photon. This is a really basic picture of the OPA process, so let's try to relax some of the previous approximations. We have not said for example how to obtain the phase matching condition. This is not trivial since, in general, the index of refraction scales monotonically with the frequencies. This means that $n(\omega_1) < n(\omega_2) < n(\omega_3)$. This implies that the two conditions of $\Delta k = 0$ and $\omega_1 + \omega_2 = \omega_3$ can not be fulfilled simultaneously. There are anyway some materials for which the index of refraction can be "chosen" to fulfill the phase matching conditions. One of the most commonly used ones are the birefringent uniaxial crystals. The structure of these materials is such that it has an axis of symmetry with all perpendicular directions optically equivalent. This axis is known as the optic axis of the material, and components of light with linear polarizations parallel and perpendicular to it have unequal index of refraction, denoted n_e and n_o, respectively, where the subscripts stand for extraordinary and ordinary. Every polarization that is in between the two will then experience an index of refraction that is equal to:

[4]If we avoided the approximation of large gain $\Gamma z >> 1$ we will obtain hyperbolic functions instead of exponential.

$$n_e(\theta) = \left(\frac{sin^2(\theta)}{n_e^2} + \frac{cos^2(\theta)}{n_o^2} \right)^{-\frac{1}{2}} \tag{3.18}$$

Where θ is the angle between the optic axis and the direction of propagation of light. The polarizations of the incoming beams can therefore be chosen so that signal and idler only experience the ordinary index of refraction while the pump sees and index of refraction that depends on the angle chosen. The phase matching condition is hence obtained by angle tuning, and this in this specific case it is called Type I phase matching[5]. In this case the PM condition is simply obtained by choosing the right angle $\bar{\theta}$ for which:

$$n_e(\omega_3, \bar{\theta}) = [\omega_1 n_o(\omega_1) + \omega_2 n_o(\omega_2)] \frac{1}{\omega_3} \tag{3.19}$$

This PM condition with collinear beams works fine in the approximation of monochromatic waves. In reality we know well that the shorter the pulse, the wider the band, so to amplify a really short pulse we would need to fulfill the PM condition for a very large range of frequencies. And this is not achievable in this way[6], maintaining the same level of efficiency. If we impose that for a certain frequencies' range $\Delta k \neq 0$, we relax another of the approximations we made and we obtain a new set of equations:

$$\begin{cases} \frac{\partial \mathcal{A}_1}{\partial z} = -ib_1 \mathcal{A}_2^* \mathcal{A}_{30}\, e^{-i\Delta k z} \\ \\ \frac{\partial \mathcal{A}_2}{\partial z} = -ib_2 \mathcal{A}_1^* \mathcal{A}_{30}\, e^{-i\Delta k z} \\ \\ \mathcal{A}_3(z) \simeq \mathcal{A}_{30} \end{cases} \tag{3.20}$$

These are the same equation of the so called quasi phase matching condition. If

[5] In the type II phase matching the signal and idler are cross-polarized.

[6] Actually it is possible via wavefront tilting but is not used so often since not easy to realize.

we solve them in the approximation of large gain ($gz >> 1$), we get:

$$I_2(z) = \frac{I_{20}}{4} e^{2gz} \quad \text{with:} \quad g = \sqrt{\Gamma^2 - \left(\frac{\Delta k}{2}\right)^2} \tag{3.21}$$

That means that the gain is reduced if the phase matching condition is not fulfilled[7]. If we consider half the gain in PM condition an acceptable compromise for our purposes we can calculate the maximum Δk that still meets this standard:

$$\Delta k \simeq 2\sqrt{ln(2)}\sqrt{\frac{\Gamma}{L}} \tag{3.22}$$

We can now also relax the monochromatic approximation, since, in practice, when speaking of wide bandwidth pulses we are already breaking it, and so the coupled equations become:

$$\begin{cases} \frac{\partial \mathcal{A}_1}{\partial z} + \frac{1}{v_{g_1}} \frac{\partial \mathcal{A}_1}{\partial t} = -ib_1 \mathcal{A}_2^* \mathcal{A}_{30}\, e^{-i\Delta k z} \\ \\ \frac{\partial \mathcal{A}_2}{\partial z} + \frac{1}{v_{g_2}} \frac{\partial \mathcal{A}_2}{\partial t} = -ib_2 \mathcal{A}_1^* \mathcal{A}_{30}\, e^{-i\Delta k z} \\ \\ \mathcal{A}_3(z) \simeq \mathcal{A}_{30} \end{cases} \tag{3.23}$$

The first dramatic effect of introducing a short pulse instead of a long pulse is that, after a while, inside the crystal, the velocity mismatch of the pulses will cause them to reciprocally spread apart. If there is no superposition of the pulses, of course, the gain goes to zero and so there is no amplification anymore[8]. Nevertheless we can distinguish between two cases (displayed in Figure 3.7): if the two mismatch are concordant the pump will stay in the middle of the two pulses, in

[7] Indeed, it is still possible to operate an OPA in these conditions but the amplification band will be reduced.

[8] In fact if even just one of the $\mathcal{A}_i$ terms goes to zero the equations decouple and so there is no positive feedback anymore.

the other cases the pump and the pulses will run away one from the others. In the

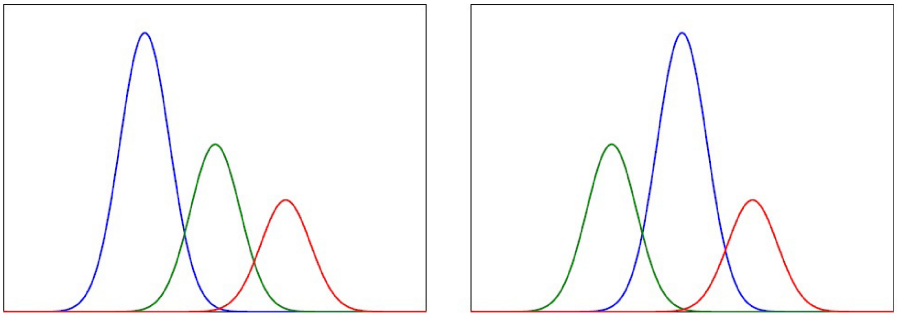

Figure 3.7: Pump (blue), signal (green), idler (red) propagating into the medium with (a) $\delta_{23}\delta_{13} > 0$, or with (b) $\delta_{23}\delta_{13} < 0$. Adapted from [5].

first case the gain efficiency still holds high since the pump can always amplify the tails of the pulses and therefore the amplification is efficient for a longer time and distance.

This said one can always enhance the OPA efficiency by making use of a Chirped Pulse Amplification setup, in which, as seen before, the input pulses are stretched, then they are amplified and then re-compressed. In this way one deals again with long pulses so there are no more problems related to velocity mismatches.

In the most general case one should also consider that the angle between the optical axis and the direction of the light inside a birefringent medium induces a reciprocal walk off between cross polarized light. This walk off acts in the same way as the velocity mismatch[9], spreading apart the beams, hence inhibiting the gain, and consequently limiting the optimal length of the crystal.

Keeping all this in mind one can try to calculate and optimize the amplifica-

[9]With the only difference that velocity mismatches acts on the direction of propagation of the pulses, while the walk off acts on the transverse direction.

tion bandwidth $\Delta\omega$. The Δk is intrinsically linked to the bandwidth $\Delta\omega$ as we already mentioned. In fact if one expand in series Δk imposing that the main effect is due to the bands of the signal and idler, will obtain:

$$\Delta k = \delta_{12}\Delta\omega - \frac{1}{2}(\mathrm{GVD}_1 + \mathrm{GVD}_2)\Delta\omega + ... \tag{3.24}$$

Where, as before, the group velocity mismatch is $\delta_{12} = \frac{1}{v_{g1}} - \frac{1}{v_{g2}}$. If we stop the expansion at the first order, and by making use of the eq. (3.22), we can get:

$$\Delta\nu_{\mathrm{FWHF}} = \frac{2}{\pi}\sqrt{ln2}\sqrt{\frac{\Gamma}{L}}\frac{1}{|\delta_{12}|} \tag{3.25}$$

If we want Δk small or, equivalently, a large bandwidth we have to impose $\delta_{12} = 0$. This can be done by introducing an angle Ω between the two pulses Figure 3.8.

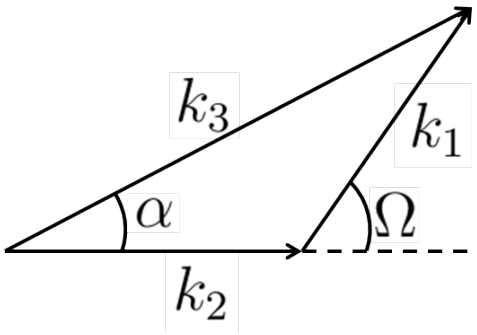

Figure 3.8: Scheme of the Non-Collinear OPA Phase Matching

Indeed, in this way one can still satisfy the PM condition and, at the same time, also match the group velocities. An OPA with such characteristics is called non-collinear (NOPA), and, after some trigonometry's calculation, one can deduce that the optimal angle for maximum bandwidth is the one for which:

$$v_{g_2} = v_{g_1} cos(\Omega) \tag{3.26}$$

So the group velocity mismatch goes to zero if the group velocity of the signal is equal to the projection of the group velocity of the idler along the signal's propagation direction. In reality the angle that we are mostly interested in is the one between the signal and the pump, since those are usually the input beams. This is anyway not a problem since it can be obtained by the other imposed conditions. Even in the case of matched velocities the output bandwidth can not be infinite, in fact it is limited by the second order dispersion mismatch. Thus the maximum theoretical bandwidth reachable in a NOPA system is:

$$\Delta\nu_{\text{FWHF}} = \frac{\sqrt{2}(ln2)^{1/4}}{\pi}\left(\frac{\Gamma}{L}\right)^{1/4}\frac{1}{\sqrt{|\text{GVD}_1 + \text{GVD}_2|}} \tag{3.27}$$

This concludes the theory's dissertation on the Nonlinear Polarization and the OPAs, a lot more could have been said about these two arguments but we decided to choose just the arguments strictly needed to approach and understand the rest of the thesis.

Chapter 4

Setup Description

4.1 General description

There is a growing interest in having a Mid-IR pulse source for different type of time-resolved pump-probe experiments. These experiments typically need a Mid-IR source in the range of 10 up to 20 μm (which is approximately 30 down to 15 THz). This is a region in which a lot of materials interesting for various reason have some phonons that can be excited or that can be observed and this is why a lot of research groups are interested in having a solid pump-probe system such the one here described.

So one of the initial requirements was to have some sort of tunability in that range of frequencies. Another key ingredient of our experimental setup was the Carrier Envelope Phase Stability or CEP Stability. When we introduced a pulse's model in the previous chapters we neglected, for simplicity, the phase term ϕ, in fact in the most general case one should write:

$$E(z,t) = Re\{\mathcal{A}(z,t)e^{i(\omega_0 t - k_0 z + \phi)}\} \tag{4.1}$$

Where ϕ is called, indeed, Carrier Envelope Phase, since it that indicates the position and eventually the shifting of the carrier wave in respect of the envelope pulse. This can be visualized in Figure 4.1.

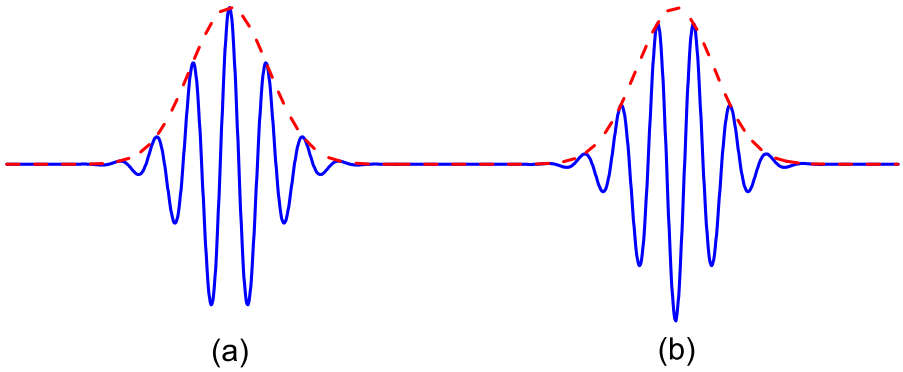

Figure 4.1: Example of Carrier Envelope Phase shift of π of the pulse (a) in respect to the pulse (b).

In principle, the CEP of a pulse traveling into a medium is constant, assuming that the intensity is low enough to avoid chirping of the pulse and any other unwanted effects[1]. But this is not true for the relative CEP of two consecutive pulses of a mode-locked laser, and we will return to this point later on.

The shot-to-shot stability of the CEP is so important since it implies the possibility of measuring the actual pulse's electric field instead of measuring just the intensity profile of the pulse. Reading the electric field trace implies having all the possible informations needed[2], some of which can be particularly hard to get otherwise. At the moment there are no technique able to detect the single shot electric field of a pulse[3]. This means that in order to acquire it one must have a lot of pulses with always the same electric field, which basically means a train of pulses with the same CEP, since the other parameters can be reasonably approximated to be constant anyway. It also crucial to have a stable CEP source in High Harmonic Generation (HHG) process and experiments, as well as in many time-resolved pump-probe experiments in which the ability to hit the samples always

[1]Which, in general, is the standard situation if one wants to work with Transform Limited pulses. And this is also why we neglected in the first place.

[2]Measuring the electric field one can derive all sort of proprieties of the pulse: eg shape, time duration, spectrum, phase etc...

[3]It is even hard to detect one of the mentioned informations of just one pulse.

with the same electric field (so well defined frequency and phase) is essential[6].

Of course there are other basic requirements for the Mid-IR source to be efficient and versatile. First of all, the power, and hence the peak intensity. Those are needed since, on first approximation, the more power, the more the material can be excited and thus respond, the more the effects can be observable[4]. Of course, if the pulse is too intense one can have all sort of problems: from chirping to self phase modulation up to damaging of the sample, but usually this is not the case. Secondly one would like to always have a Transform Limited therefore un-chirped pulse. In fact a TL pulse has the minimum time-duration associated to a particular bandwidth, and that gives the maximum temporal resolution as well as the maximum peak intensity. Moreover, as we already mentioned, it is usually easier to stretch a pulse then to compress it.

As one can imagine there are a lot of other different features than need to be fulfilled to obtain a perfect source for an experiment, some of which also change from experiment to experiment. So this implies good tunability of the system in general and good control over all the processes and, in particular, an excellent capability of measuring the output pulse's proprieties. On top of that, since some of the experiments can last as much as 2 or 3 days the system needs to be super-stable over a long period of time, and, of course, the reproducibility of the output has to be high.

Another important parameter that we were trying to optimize during the construction of the system was the space occupied by the optical apparatus, since we wanted it to be quite compact so that it could be placed on a board and then moved when necessary. This resulted to be more complicated than imagined.

Keeping all these parameters in mind and looking at the state of the art

[4]In the case one wants to use the Mid-IR as a probe and the power is too high there is always an easy solution to trash away some extra power.

systems we decided to build our Mid-IR source as sketched in Figure 4.1.

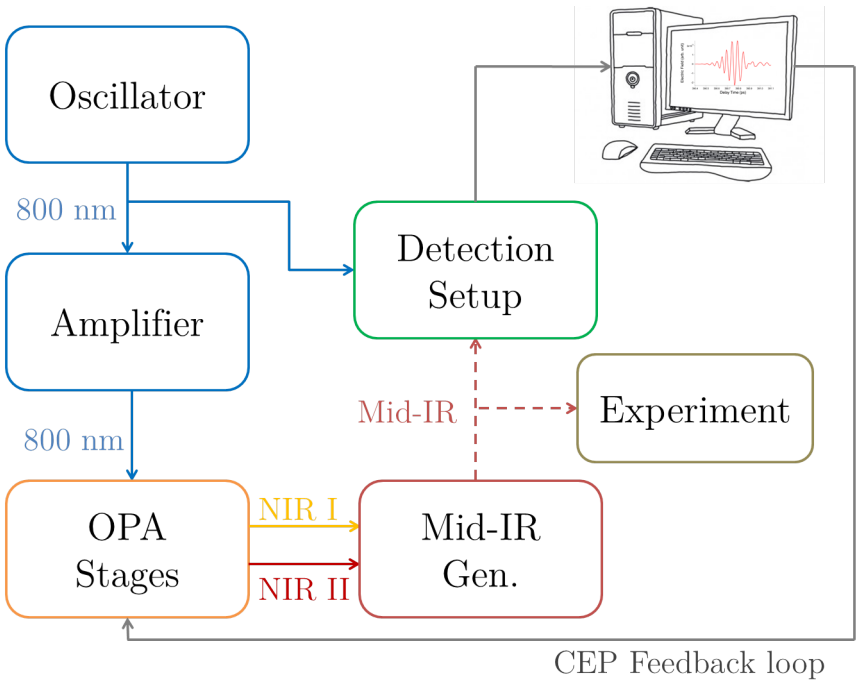

Figure 4.2: Scheme of the setup. Mid-IR Gen. stands for MidInfraRed Generation Setup.

Starting from the top we have a commercial oscillator bought from Coherent and called Vitara. This is a 500 mW, 800 nm central wave, 80 nm wide[5], 13 fs short, 80 MHz repetition rate mode-locked Ti:S oscillator. This is a quite standard product and it is primarily used to seed the amplifier.

The Amplifier is a CPA mode-locked regenerative[6] Ti:S Amplifier bought from Coherent as well, and called Legend. This optically pumped amplifier, seeded by the oscillator, generate up to 5.5 W at 800 nm, 13 nm of bandwidth with 1 KHz repetition rate and pulses time duration of roughly 90 fs.

[5]Here, and from now on we will postulate that every temporal or spectral bandwidth measurements or data we will refer to is always to consider as Full Width at Half Maximum (FWHM), unless otherwise indicated.

[6]This means that the cavity is controlled by two Pockels cell that enable the seeding pulse in and after a certain number of round-trip allow the output pulse out.

We chose the Ti:S regen. amplifier for its well known stability, and reproducibility. The power output was chosen to fit the experimental pump-probe setup power requirements and also keeping in mind that we needed a good repetition rate to be able to perform the experiments as quickly as possible[7]. Indeed the repetition rate and power output are reciprocally limited, and the limit is imposed by the maximum total energy that can be store inside the active region.

The pulse generated by this kind of lasers is generally close to the Transform Limit, but it can be tuned thanks to the remote control on the compressor. We had no need of a very wide bandwidth nor we needed a very short pulse, indeed, as we mentioned in the previous chapters, the OPAs work better with long pulses or, in the same way, relatively narrow bandwidth. This said we always tried to stay close to the TL since otherwise we would generate non-TL Mid-IR[8]. Of course a quite long pulse helps with avoiding non-linear effects such as Self Phase Modulation (SPM) in air as well as in the crystals, that is always much appreciated.

Actually not all the power generated by the Amplifier is sent to the OPA stages, roughly 1 Watt is deflected through a beam splitter to be used in the probe setup, or for other miscellaneous usages.

One of the most common way to generate Mid-IR in the region of interest is to perform difference frequency of two Near InfraRed (NIR) beams in a well suited crystal. As already discussed, the Difference Frequency Generation (DFG) is a process in which two incoming beams generate a third beam which has a frequency that is the difference of the two first beams. It is quite clear that if we can tune a bit the frequency of the first two, then we will tune consequently the frequency of the generated beam. In Figure 4.3 is a reminder of the DFG process.

So the two NIR beams are generated thanks to an OPAs setup and then they are

[7]Indeed more pulses per second means more informations in the same time, therefore less time needed to perform an experiment.

[8]And we need a TL Mid-IR pulse since it gives the maximum peak power, needed to pump the material properly especially when dealing with non-linear phenomenas.

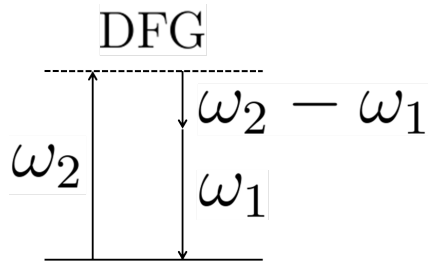

Figure 4.3: Difference Frequency Generation sketch.

send to the DFG stage. The Mid-IR generated there is hence fully characterized by a detection setup, before steering it to the experiment. The OPAs setup is designed to obtain two NIR beams that will generate an intrinsically CEP stable Mid-IR, but in the real world this is true only to some extend. So the detection scheme is used also to implement a feedback loop, controlled by a computer program and running in parallel to the experiment, that actively acts to maintain the CEP stability of the system.

4.2 Opa Setup and Passive Stabilization

We will now describe the setup needed to generate the two NIR beams. To convert our 800 nm source in the two needed beams we make use of two Optical Parametric Amplifiers. We already described the general solution for such device and, under certain approximations[9] the result is the one shown in Figure 4.2

$$\begin{cases} I_1(z) = \frac{I_{10}}{4} e^{2\Gamma z} \\ I_2(z) = \frac{I_{20}}{4} e^{2\Gamma z} \\ I_3(z) \simeq I_{30} \end{cases} \tag{4.2}$$

[9]Even if this result is strictly valid only for perfectly phase matched conditions, we demonstrated that it is possible to obtain a certain degree of phase matching thanks to birefringence and non collinear schemes. In these cases the representation given here is still valid, just taking into account a reduction of the theoretical gain when moving out of the central wavelengths (the one for which we imposed the PM condition).

Those are respectively the intensities of the signal, the idler and the pump pulse. So we need a seeding beam, to have an initial intensity value different than zero, otherwise the first two equations have just the trivial solution. In principle even just the zero-point oscillations of the electric field can be exploited to generate the needed beams, but, first of all, this process is not really efficient and, secondly, it is quite hard to impose the phase matching condition needed to select the right frequencies. So we need a seeding beam that can give us some initial intensity to amply it more efficiently. The trick usually consist in generating a low-power continuum bandwidth from which one can select the sought frequencies imposing the right angle to fulfill the PM condition for those particular frequencies.

The effect exploited in this case is the super-continuum white light generation in a crystal. This complex phenomenon it is mainly due to self-focusing and self-phase modulation. We already talked about self-focusing in the previous chapters, and we introduced the following notation: $n = n_0 + n_2 I$. The same formula leads to the so called self-phase modulation just observing that:

$$n(t) = n_0 + n_2 I(t) \tag{4.3}$$

$$E(z,t) = Re\{\mathcal{A}(z,t)e^{i(\omega_0 t - kz)}\} \tag{4.4}$$

but:

$$k = \frac{\omega_0\, n(t)}{c} \Longrightarrow k = \frac{\omega_0\, (n_0 + n_2 I(t))}{c} \tag{4.5}$$

So, if we now calculate the instantaneous frequency $\omega_i(t)$ of the pulse of the previous equation we obtain:

$$\omega_i(t) = \frac{d}{dt}\left[\omega_0 t - kz\right] = \omega_0\left(1 - \frac{n_2}{c}\frac{dI(t)}{dt}z\right) \tag{4.6}$$

This means that new frequencies are generated hence the spectrum is broadened in both direction. Indeed the pulse temporal shape is so that the situation is always similar to the one sketched in Figure 4.4.

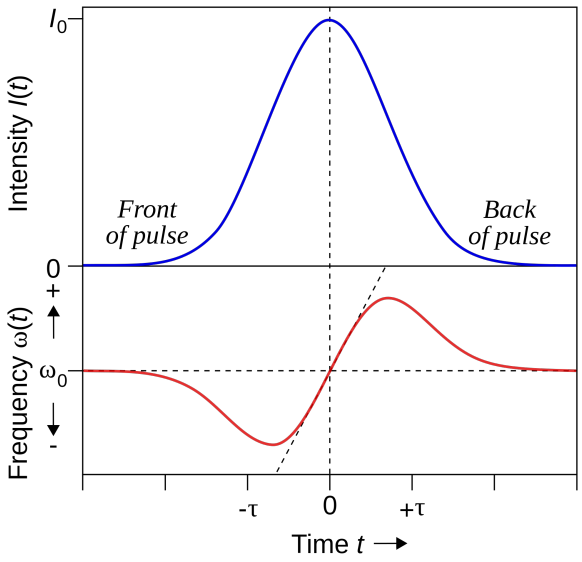

Figure 4.4: An increase in intensity causes a red shift in the front of the pulse while a decrease in intensity causes a blue shift in the back of it. Image by Bob Mellish from [7].

This effect is highly enhanced by the self-focusing, since that induce a tightening of the beam, hence a higher derivative. And that can explain why focusing tightly a pulsed beam onto a relatively high $\chi^{(3)}$ crystal produces a very broad spectrum,often called white-light[10]. In our case the crystal was a few mm thick sapphire crystal and of course the focused beam was 800 nm. This was enough to generate some seeding light in the region needed for our OPAs to work properly, that is from around 1 μm up to 2 μm.

[10]The name comes from the usual color visible by the naked eye.

Since the white-light generation process is highly non selective, it is not very efficient in generating a NIR beam of reasonable power, hence only a negligible amount of power coming from the amplifier is used for this [11]. On the other hand, the OPA process, as we already discussed, is more efficient but, nevertheless, it is usually better, if possible, to divide the NIR generation process in two stages of OPA. The first, responsible for the selection from the WL of the chosen frequencies but generating a beam of medium power, then, the second, that amplify greatly the initial beam to quite high power.

Taking all that into account and a lot more from the literature and the state of the art systems we designed an OPAs scheme as it is in Figure 4.5.

One may notice that here, not only we used two stages, but we actually used two separate lines, each one designed to produce a single NIR beam. In principle one could just tune one single double stage OPA to produce a signal and idler whose difference in frequency is the one necessary for the Mid-IR. In the case of interest we just took the signals and "trashed" the idlers out of every single stage[12]. Of course this is not a very efficient move, but there are two main reasons why we did it: on the one hand it makes the tuning of the system easier and therefore faster, but also, on the other hand, it is the way to intrinsically lock the Carrier Envelope Phase of the Mid-IR.

Indeed, for unsaturated DF mixing of two pulses with CEP respectively of ϕ_1 and ϕ_2, the resulting pulse has an overall phase ϕ_{DFG} of:

[11] Indeed, even if the process need a high intensity beam, this can always be possible making sure of focusing the beam tightly enough. And this is quite easy using a short focus lens.

[12] With a further implementation of the system one could actually make good use of the idlers just steering them out. It can be done quite easily, just placing some mirrors in the system and finding a free path for them out, but we did not bother with that since at that time we had no use for them. They could even be used to generate another CEP stable Mid-IR of the same frequency as the first one, but it is a bit more complicated mostly due to some practical restrictions, so we did not implemented it.

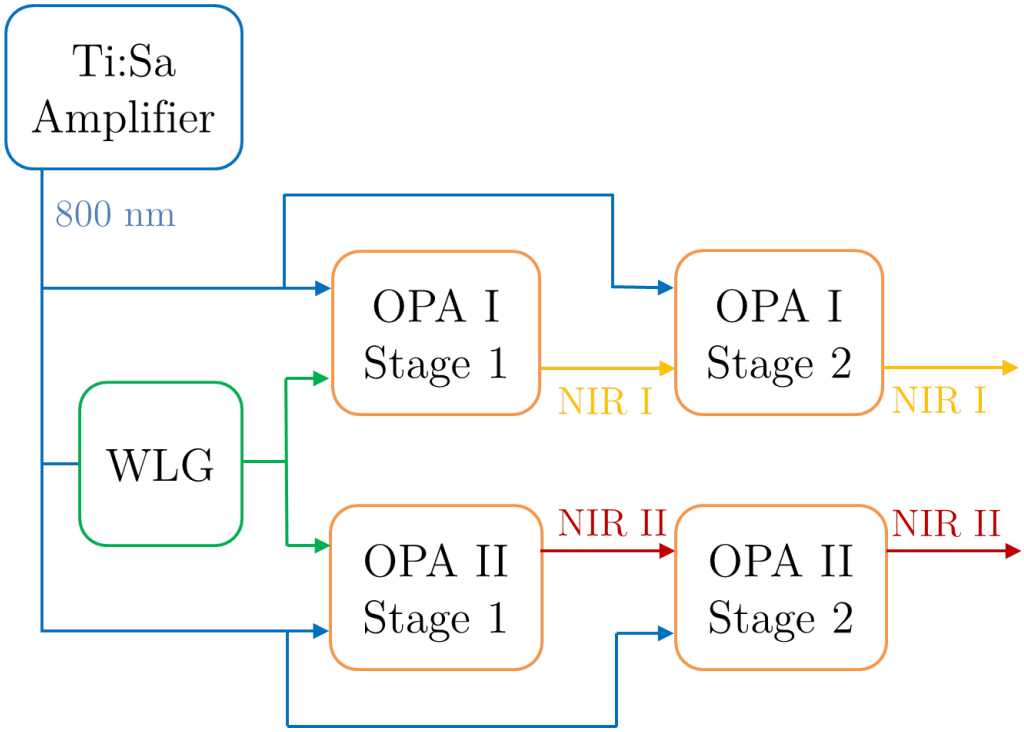

Figure 4.5: Scheme of our OPAs setup. WLG stands for White Light Generation.

$$\phi_{DFG} = \phi_1 - \phi_2 - \frac{\pi}{2} \tag{4.7}$$

This said if the two pulses are generated from the same broadband super-continuum then they will have mutually locked phase, so:

$$\phi_1 = \phi_2 + \Delta\phi \tag{4.8}$$

Where, $\Delta\phi$ is a constant. So the CEP phase of the DF pulse will be constant:

$$\phi_{DFG} = \phi_2 + \Delta\phi - \phi_2 - \frac{\pi}{2} = \Delta\phi - \frac{\pi}{2} = const. \tag{4.9}$$

So this means that mixing the two signal derived from the same WL and amplified

in the OPAs result in a CEP stable DF pulse, hence, in this case, a CEP stable Mid-IR. If we had used the signal and idler coming from the same OPA we would obtain a ϕ_{DFG} that is:

$$\phi_{DFG} = \phi_S - \phi_I - \frac{\pi}{2} = \phi_P + const. \tag{4.10}$$

Where S stands fro signal, I stands for Idler and P for pump. Therefore the DF pulse generated will have a phase related to the pump of the OPA, that is the Ti:Sa laser pulse. But the Ti:Sa laser, being a mode-locked laser is not intrinsically CEP stable. In fact every round-trip of the cavity induce a phase shift of several radiants, which, in general, will not be equal to an integer multiple of $2pi$, that means that every pulse of the train coming out of the laser will have a CEP different than the one before. There are CEP stabilized Ti:Sa laser but they have a lot of other constriction and this was anyway not our case.

There are a lot of other practical and experimental reason for which the real scheme is a lot more complicated that the one showed before. For example, every mixing process (OPA, DFG) needs a translational stage mounted on one of the two beam path to be able to finely tune the path length of that one beam in respect to the other in order to perfectly match the two. Another aspect that has to be carefully issued is the size matching of the beams in these mixing process. Once again the sizes of the two beam mixing at every stage of the system need to be equally the same, to maximize the efficiency of this processes. Not only, indeed, the beam size, is a particularly important feature that need to be addressed with careful attention in general. We would like the beams always to be quite unfocused, so with a big size, to avoid every unwanted non-linear process in air as well as inside and onto the optics. And, of course, the more the beam are powerful, the more they need to be maintained big. But the optics itself and general

hindrance issues ask for a moderately small beam size. So we were forced to use some telescope in transmission, as well as in reflection to adapt the various beam size according to all these issues. Since the system has to be quite flexible and tunable one has to be able to make some adjustment, for example tuning the PM angle of an OPA to a different value to change the generated wavelength, without compromising the alignment of all the optics in cascade. For this reason two iris and two adjustment mirrors were always following the most touched optics on the beam-path of that beam. There were then particularly designed optics to treat the polarization of light accordingly to the needed usage, and specifically used to optimize PM (as we already discussed). Then some beam-splitters were used to rightly distribute the beam power to the different stages for optimal efficiency. For example, the first OPA's stages demanded for low-power pump, unlike the second stages, so almost 90 per cent of the power was split to be steered into this second stages. When we needed to separate beam of different frequencies we made use of some dichroic mirrors, in which one beam of a certain frequency is reflected while the other passes through[13].

Hence the real scheme of the system looks more like the ones in Figure 4.6 and Figure 4.7.

On Figure 4.6 the black box is the actual breadboard on which the OPAs setup are build so they can be eventually moved. DM stands for Dichroic Mirror, PBS for Polarizing Beam Splitter. The light blue little rectangles represent the mirrors, the double arrows the translational stages and whenever there is a percent mirror that is a beam splitter. In and Out are the entrance and exit of the beams in respect of the breadboard. Blue beams are 800 nm ones, green are WL supercon-

[13]They are practically dielectric mirrors with the usual high reflection coated front surface to reflect a narrow bandwidth of frequencies and an anti-reflection coated back surface to let the non reflected beam pass through. The coatings, as in Bragg reflector, are multi-layers of low and high index materials.

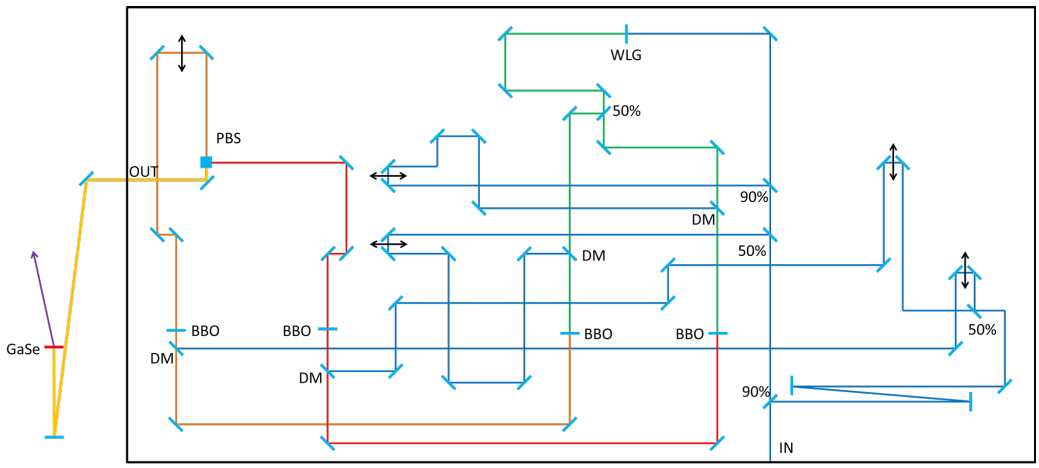

Figure 4.6: Medium Detailed Scheme of the OPAs and DFG setup.

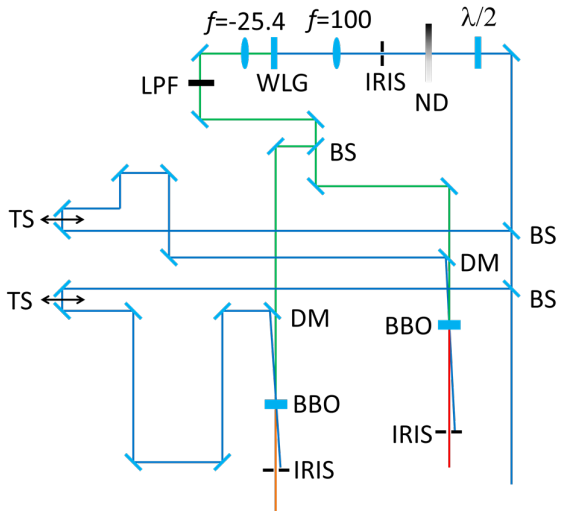

Figure 4.7: Full detailed scheme of the WLG and first stage OPAs. TS stands for translational stage, ND for Neutral Density filter, LPF for Low Pass Filter, BS for Beam Splitter, $\lambda/2$ is a half-wave plate and near every lens there is its focal length.

tinuum beams, red, orange and yellow are NIR beams, and the violet arrow is the Mid-IR. BBO stands for Beta Barium Borate[14] which is the birefringent crystal we chose for the OPA processes, while GaSe stands for Gallium(II) Selenide which is the one for the DFG. Although all of this is really important for the system to work well, from here on we will not bother with this level of detail anymore, unless it is strictly necessary, since it is not really interesting for the purpose of the Thesis.

The routine Mid-IR wavelength for our experimental purpose was around 15 μm. Our OPAs work in the region of 1000 up to 2500 nm. For purely practical/experimental reason we chose to work in the region of 1200 up to 1400 nm[15]. So, this is also why we were forced to use the signals instead of the idlers (for example they will not be visible onto a paper sheet.). For reasons we already discussed we used a non collinear geometry for the first stages. The result spectra of the first stage OPAs are shown in Figure 4.8 and 4.11. We conventionally called OPA1 the beam with less photon energy (i.e. longer wavelength), and OPA2 the other. The crystals chosen here were 3 mm thick type II BBOs.

So we had an OPA set to 1350 nm, with FWHM bandwidth of 43 nm and 10 mW average power with fluctuations around 1% [16]. The, so called, second OPA was set to 1235 nm, 64 nm wide, 11 mW of average power and again around 1% fluctuations. These are the results of pumping each OPA with approximately 150 mW.

Those are the routine wavelengths in our setup, of course when one wants to tune the Mid-IR wavelength, they has to be tune to match the requirements.

[14]Whose chemical formula is $Ba(BO_2)_2$. There are two stable phases for the crystalline structure of this material, called alpha and beta. Only the second one is non-centric symmetric, so it is the only one interesting for our purposes.

[15]In fact the two photon absorption of these beam onto a white paper makes us able to see the beam. This because this absorbed light can be remitted and it is now in the visible region (600 up to 700).

[16]This is calculated dividing the standard deviation by the average power measured on a 5 minutes log.

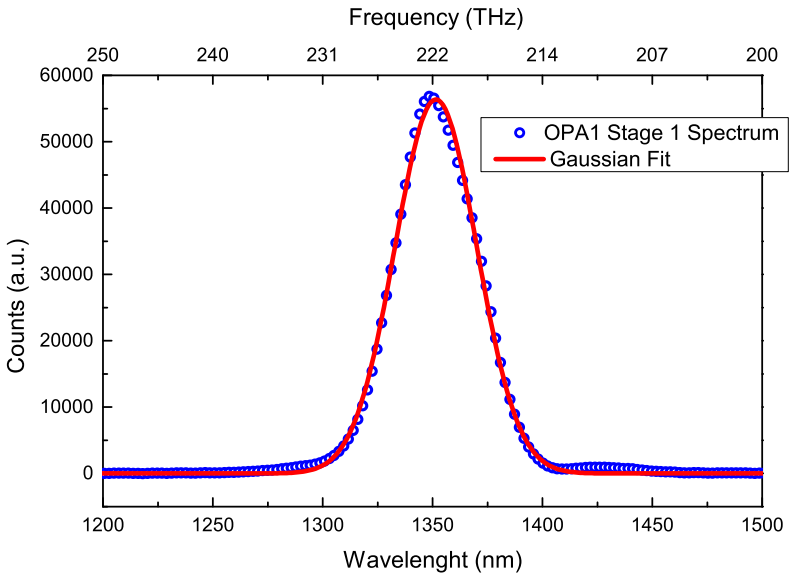

Figure 4.8: Signal's Spectrum of the first stage (OPA1)

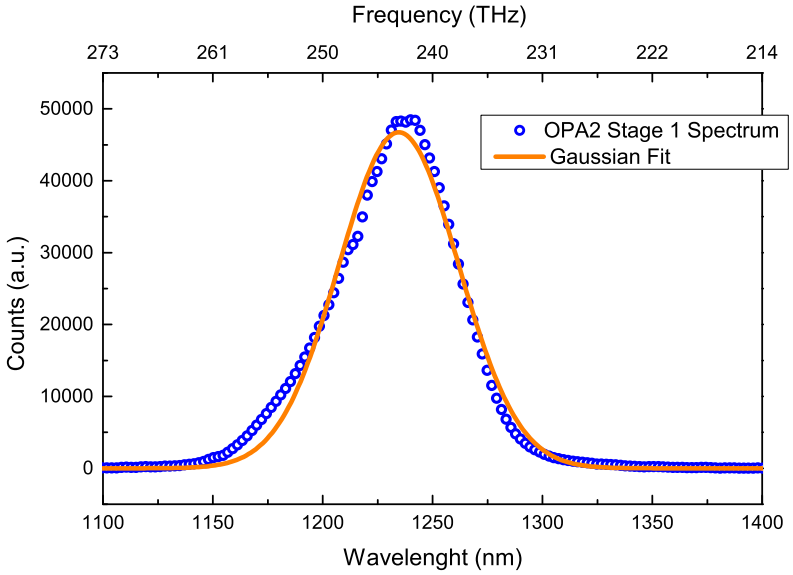

Figure 4.9: Signal's Spectrum of the first stage (OPA2)

The second stage were pumped with 2 W each but we used a collinear scheme in this case. Indeed we are not interested in having a large bandwidth, and the crystal itself is not particularly long[17], so the velocity mismatch effects are not exceedingly dramatic. Hence the gain is still moderately high for the portion of bandwidth we are interested in. The reason why we do not want a large bandwidth NIR pulses is because then it would be quite difficult to obtain a narrow enough spectrum of the resulting Mid-IR difference frequency beam. Moreover it is easier with such powerful beams, since they must have a quite big spot-size, to separate the signal from the idler and the pump with a dichroic mirror instead of spatially block them, as we did in the first stages. In Figure 4.10 and 4.11 we show the two second stage spectra.

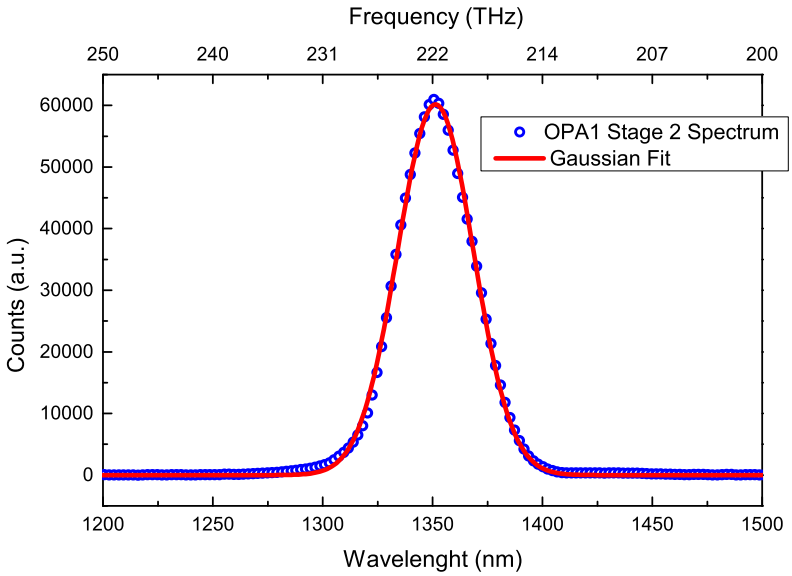

Figure 4.10: Signal's Spectrum of the second stage (OPA1)

The central wavelength of the first OPA is again 1350 nm, 40 nm wide and roughly

[17]We used 2 mm thick type II BBOs, which are short enough to still avoid pump depletion, which leads to unwanted effects on the generated NIR pulses.

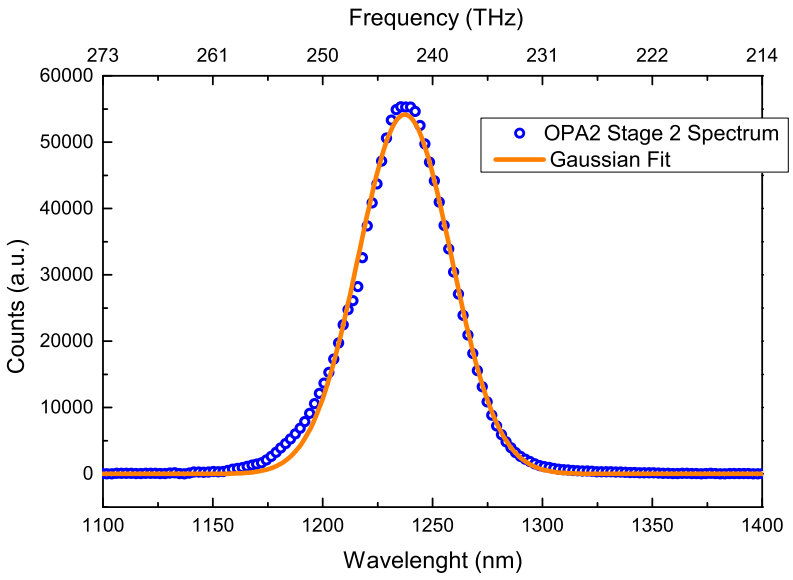

Figure 4.11: Signal's Spectrum of the second stage (OPA2)

350 mW average power, and again power fluctuations within 1%. The second one at 1235 nm 49 nm wide, with identical power features as the first one (350 mW, 1%). The general power efficiency of this stage of the system is around 15,5%, which, taking into account that we are dealing with non-linear processes, is quite high. We were able to reach even higher power figures with second stages up to 500 mW each, but this was done pumping probably too hard on long BBOs crystal and that turned into a poor quality beam. Pumping hard, in this scenario, means tightening up the beam-size, which, as we know, increase the beam intensity and enhance the efficiency of the non-linear processes. This means that also higher than second order non-linear phenomena can show up, which can mess up badly the spectrum and the beam shape. One example of these unwanted spectra is shown in Figure 4.12.

So we decided to settle for the above mentioned power figures, which are a good compromise between quality and power. This concludes the description of the OPAs setup, since, after the second stage amplification, the two signals of the

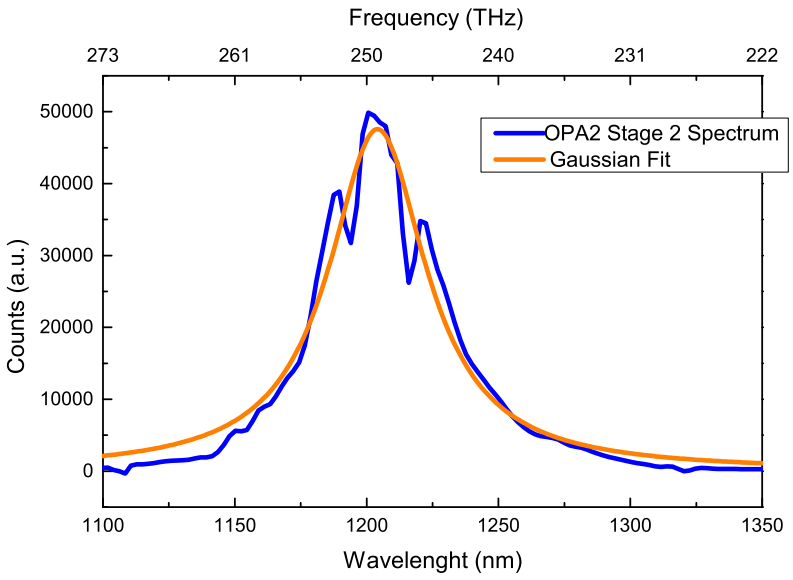

Figure 4.12: Bad looking spectra obtained with a long BBO crystal pumped too hard. It is easy to catch the difference between this and the previous ones.

OPAs are combined with a given angle to converge on the same optics and to be send to the Mid-IR DFG crystal. To change the frequency of the Mid-IR one has to tune the NIRs in a way to change the difference in frequency of the two. In our case we used to maintain the second OPA fixed to the wavelength above displayed and just tune a bit the angle of the first OPA (on both stages) to adjust its wavelength to obtain the needed Mid-IR wavelength in the difference frequency generation.

4.3 Mid-IR Generation Setup

We will not discuss too much in detail the theory of the DFG, since, as already mentioned, is practically the same as the one of the OPA phenomena. We will instead talk about one of the main problem with having a wide tunable Mid-IR sources, which is to find the right generation crystal. Indeed, it has to work well with non-linear processes, but also it has to be transparent in the region in which we are interested to work. In fact, the non-linear processes that we

discussed occur between virtual energy levels, if absorption is involved this effects are suppressed. The single crystal GaSe chosen for the purpose not only has a large non-linear coefficient and a high damage threshold but also a quite wide transparency range as one might see from Figure 4.13. So, in principle, with this crystal one can generate Mid-IR in the region of 2 μm up to almost 18 μm. Of course, the efficiency follow the transmission, so the lower is the transmission the lower will be the efficiency. There are a number of other crystal that one might consider to use instead of the GaSe. We chose this because, all considered, it is one of the best commercially available crystal of this kind.

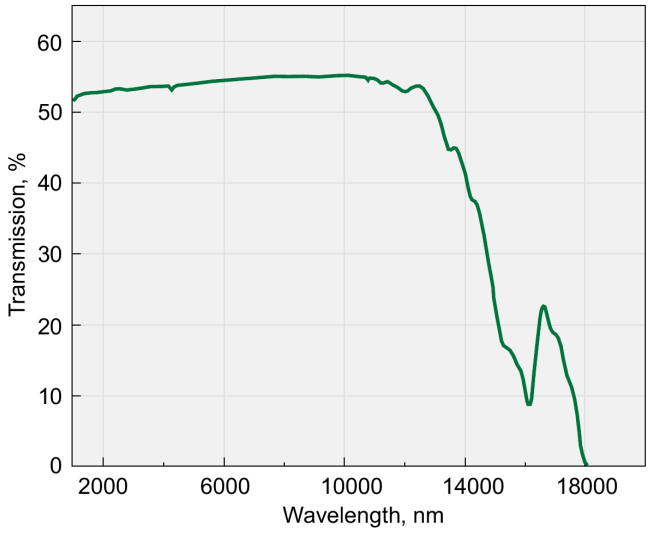

Figure 4.13: Transmission spectra of 17 mm long uncoated GaSe crystal. Courtesy of eksmaoptics.com[8].

Another key parameter to optimize is the length of the crystal itself. The longer it gets the more powerful the Mid-IR comes out, but, at the same time, the NIR pulses as well as the Mid-IR itself get stretched and dispersed, which is an unwanted feature. Not only, in fact, longer crystals lead to higher percentage of absorption. For example, looking at the Figure 4.13 one can imagine that if the same measurements had been done with a crystal half thick, the transmission

figures would have been quite higher. Of course the most critical part of the spectrum is the lowest transmission's one, so to obtain a Mid-IR in that region one is forced to use a relatively thin crystal in order to avoid the total lost of power due to the absorption. We had tried different length and the power results are shown in Figure 4.14.

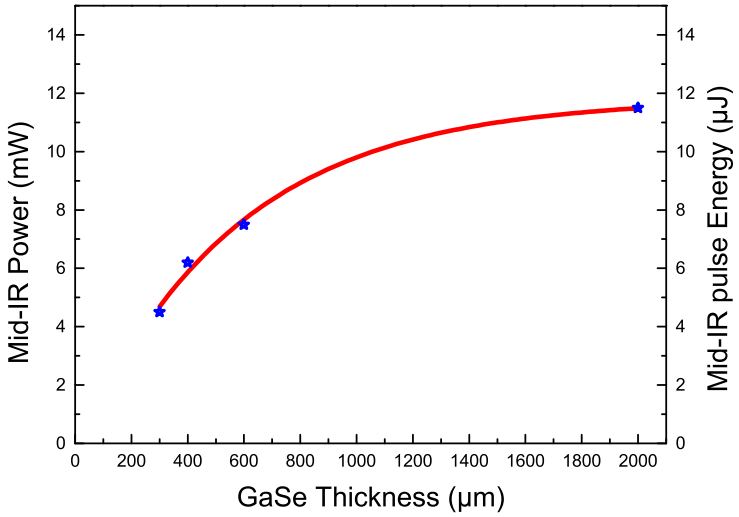

Figure 4.14: Mid-IR power measures with different GaSe crystal thickness. The blue stars are the actual measurements while the red line is simply a fitting curve. The measurements are done with wavelength around 14 μm.

One might expected to see an exponential growth of the pulse power as predicted by the most simple equations from the theory (e.g. eq. 3.17)[18]. In the real world there are some phenomena, already discussed in the previous chapters, that limit this growth. Indeed, even the most initial part of the fitted measurements curve appears to be almost linear and then saturate to a certain value. In our case this value was about 12 mW. To obtain that we could have use the same 2 mm thick crystal of the measurements but this would have limited our tunability

[18]One may argue that with so little points the fitting is totally arbitrary. The truth is that it can, indeed, be supported by some theoretical arguments, and hence we will consider it valid.

range up to about 14 μm due to the cut caused by the absorption, which was not acceptable. Evidences of the reasoning here presented can be found in the literature, for example Figure 4.15[9] show temporal traces and relative spectra of pulses generated with crystals of different length. It is easy to notice that with longer crystals, not only the pulses get longer but the spectra become narrower and it is more difficult to reach longer wavelength (e.g. lower frequencies), due to the sharp absorption cut.

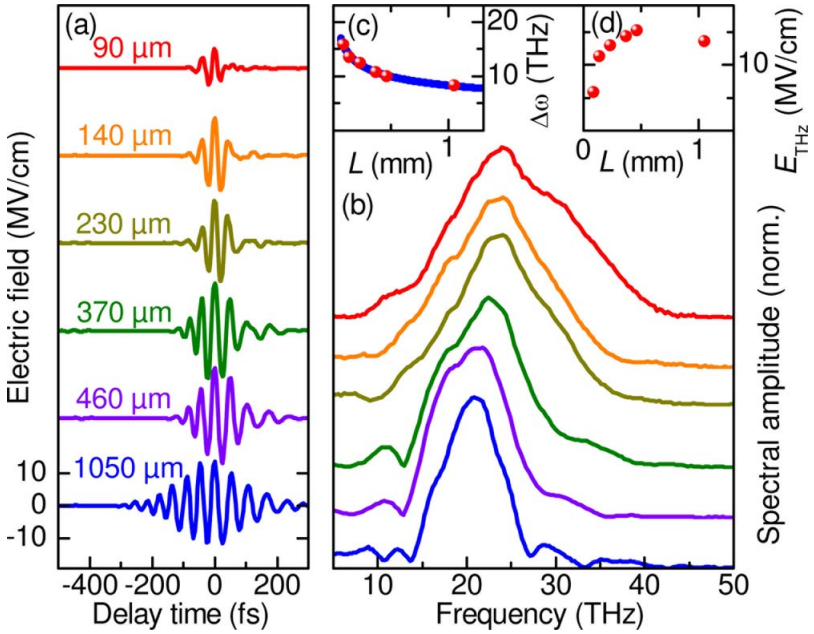

Figure 4.15: From [9] (a) Transients and (b) corresponding amplitude spectra from GaSe crystals with varying length L as indicated to the left. (c) Bandwidth $\Delta\omega$ of the measured amplitude spectra (circles) as a function of L. Solid curve, numerical fit of $L^{-1/4}$ dependence due to residual GVD mismatch. (d) Peak electric fields as a function of L.

In addition to this already quite exhaustive study, in Figure 4.16 we show our best result with the 2 mm crystal. This is centered around 20,5 THz, which is 14,6 μm. As expected the pulse is quite long and the spectra very narrow. This leave us with no possibility to maintain a good spectral weight in the region of 15 THz, which would be a desirable feature. So for all this and some other practical

reasons we finally decided to adopt a 600 μm thick crystal, which seemed to us a good trade-off between power concerns and spectral requirements.

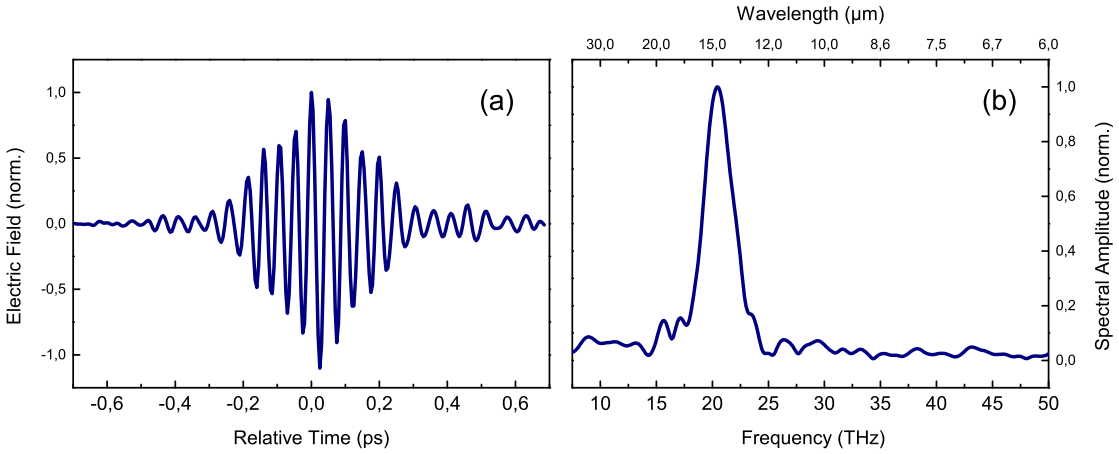

Figure 4.16: (a)Temporal trace and (b) spectrum of a Mid-IR pulse generated with 2 mm thick GaSe crystal.

With this crystal we were capable of generating pulses of good shape and temporal duration with quite wide range of tunability. In Figure 4.17 there are some Mid-IR traces and spectra obtained with NIR pulses set to various frequencies. The pulses can be generated from 15 THz (18,7 μm) up to 30 THz (down to 10 μm), they have nice shapes and good spectra. Comparing the pulse in Figure 4.16 with the (b) in Figure 4.17 one can appreciate the improvement of using thinner crystal. Indeed the pulses all look good and they still have quite reasonable power, from 5 up to 10 mW going from 15 towards 30 THz respectively. This means having 5 up to 10 μJ average energy per pulse, since we work at 1 KHz repetition rate. We could go even higher than 30 THz but then the detection scheme has some troubles to perfectly reproduce the electric field[19].

[19]One could easily change some optics in the detection scheme and work at higher frequencies, but we are not interested in doing that since the optical range is already good enough for us.

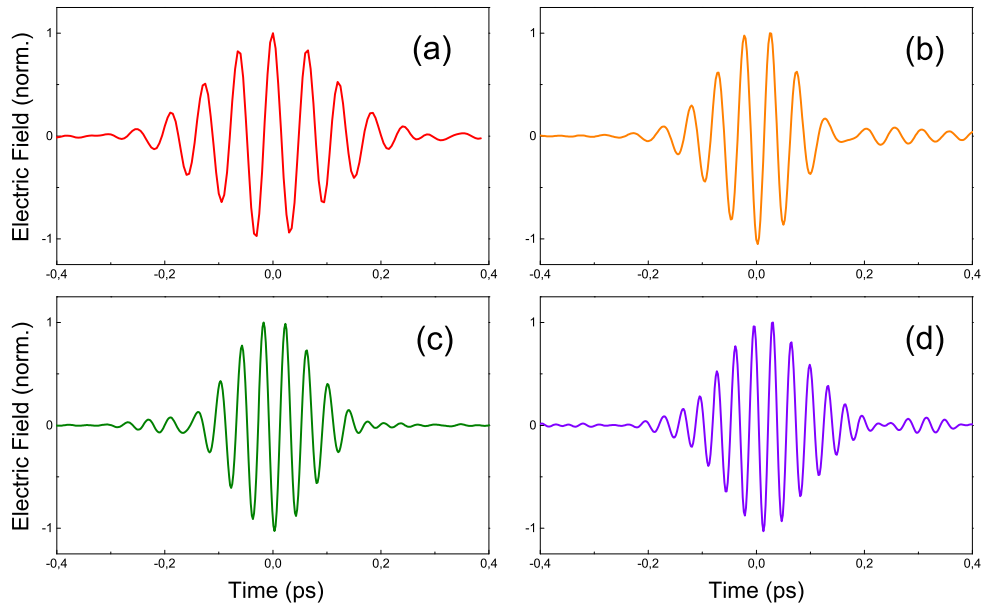

(a) Electric field's temporal trace of (a) 16, (b) 20, (c) 25, (d) 30 THz Mid-IR pulse.

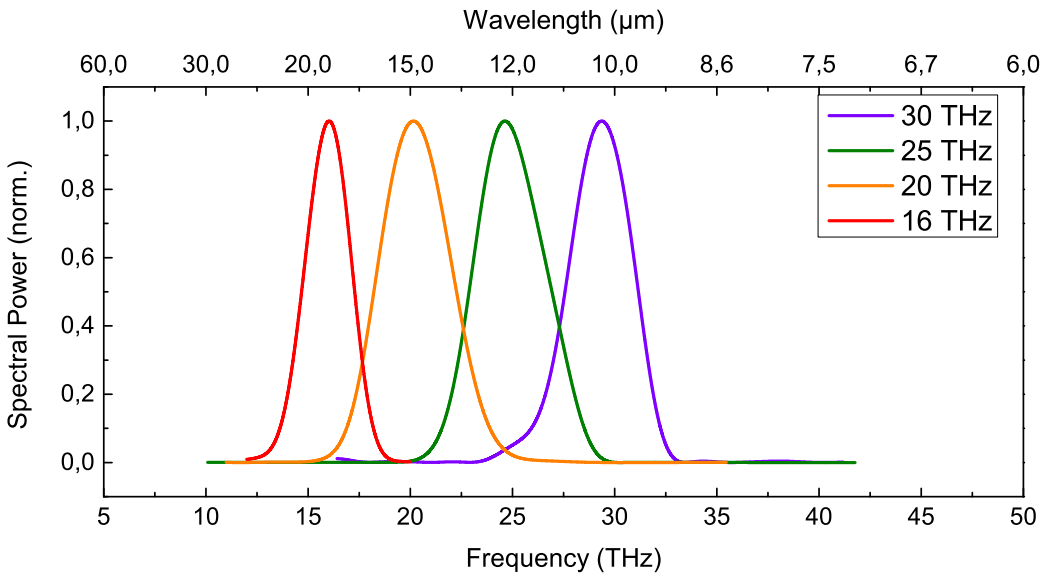

(b) Normalized power spectra computed from the above electric field traces.

Figure 4.17: Measured electric field's traces and relative power spectra of some Mid-IR pulses.

Chapter 5

Detection Setup and Narrowband Mid-IR

5.1 Electro Optic Sampling

In the previous section we showed some electric field traces of our Mid-IR pulses. Those traces are measured with a detection setup that is called Free-Space Electro Optic/Optical Sampling (EOS). This is a clever scheme that, exploiting the so called Electro-Optic effect (or Pockels effect), can trace the electric field of THz pulses[1]. Let's suppose to have two electric fields one of which is almost constant E_0 and a much shorter probe pulse E_ω often referred to as gate pulse. From the previous theoretical reasonings we earned the right to write[2]:

$$E(t) = E_{(0)} + E_{(\omega)}e^{j\omega t} + c.c. \tag{5.1}$$

$$P = P_L + P_{NL} \tag{5.2}$$

$$P_L = \epsilon_0\chi_{(0)}E_{(0)} + \epsilon_0\chi_{(w)}E_{(w)}e^{j\omega t} + c.c. \tag{5.3}$$

$$P_{NL} = \epsilon_0\chi^{(2)}E(t)^2 = \epsilon_0\chi^{(2)}\left[E_{(0)} + E_{(\omega)}e^{j\omega t}\right]^2 \tag{5.4}$$

$$P_\omega = \epsilon_0\left[\chi_{(\omega)} + 2\chi^{(2)}E_{(0)}\right]E_{(\omega)}e^{j\omega t} + c.c. \tag{5.5}$$

[1] In this text the definition THz field is used to denote the Mid-IR pulse.
[2] That is valid only for non centro-symmetic crystals.

Where P_ω is only the polarization that still vibrates at ω, and we ignored the wave-vector exponentials as well as higher than second order non-linear factors. But, in absence of the $E_{(0)}$ field, we know that:

$$n^2 = 1 + \chi_{(\omega)} \tag{5.6}$$

When the $E_{(0)}$ is present the refractive index will hence change into:

$$(n + \Delta n)^2 = 1 + \chi_{(\omega)} + 2\chi^{(2)} E_{(0)} \tag{5.7}$$

This means that in the presence of an DC electric field the index of refraction of the material change and the probe pulse propagating into that material will experience a field-induced birefringence[3]. This is what is normally called Pockels effect. In our case, if we use a probe significantly shorter than the period of the Mid-IR, and if the phase velocity of the latter matches the group velocity of the gating pulse, then we can still picture the Mid-IR as a DC field in respect to the probe itself. In the most commonly used eletro-optic crystals, among which the GaSe, the velocities happen to match for gating pulse in the region of 800 nm. In the presence of a THz field, therefore, a linearly polarized optical probe pulse becomes slightly elliptically polarized as it travels through the crystal. The ellipticity will then be proportional to the Field intensity in the same way the Δn is (see eq. 5.7).

Sketched in Figure 5.1 there is a typical EO Sampling setup. After traveling into the electro-optic crystal and eventually getting an elliptical polarization the

[3]The actual theory is a bit more complex and take into account the tensor nature of the susceptibility and from that one can deduce that the induced polarization is actually perpendicular to the probe and THz field.

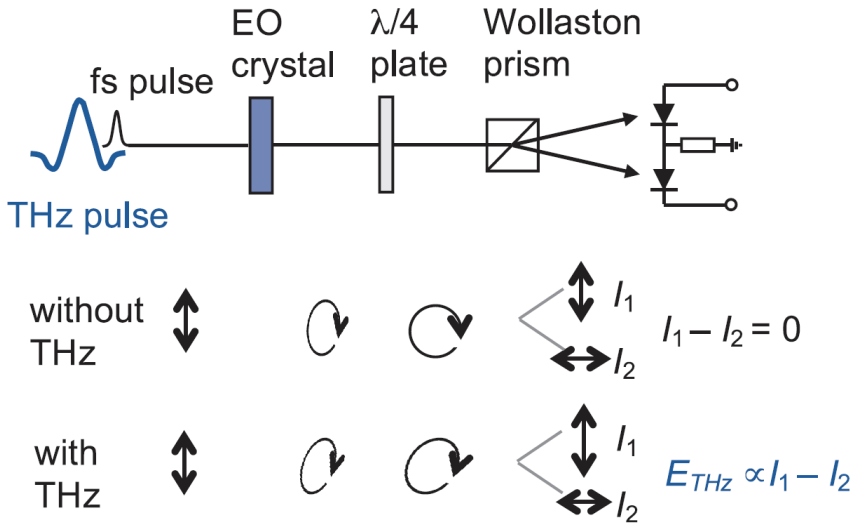

Figure 5.1: From [10]. EOS setup scheme and working principle graphical description.

probe beam passes through a quarter-wave ($\lambda/4$) plate followed by a Wallaston prism, which splits it into two orthogonal linearly polarized beams. The system is calibrated in absence of the THz pulse, adjusting the angle of the $\lambda/4$ in order to compensate for an eventual intrinsic birefringence of the EO crystal[4] and so obtaining a perfectly circular polarized pulse after the $\lambda/4$ hence a perfectly balanced detection on the two diodes. When the THz is present the light coming out of the $\lambda/4$ will not be perfectly circular polarized and therefore the detection will be unbalanced. Reading the difference of the signal coming from the two diodes one can sample the THz intensity as shown in Figure 5.2. By varing the relative time delay between the probe and the Mid-IR pulse, the temporal trace of the pulse can be mapped. It is now obvious why the CEP stability of the Mid-IR is so fundamental for this setup, in absence of that the phase information would have been lost.

The issues afflicting this kind of process are mainly related to the crystal pro-

[4]Most of the crystal used in EOS setup are already birefringent, GaSe included.

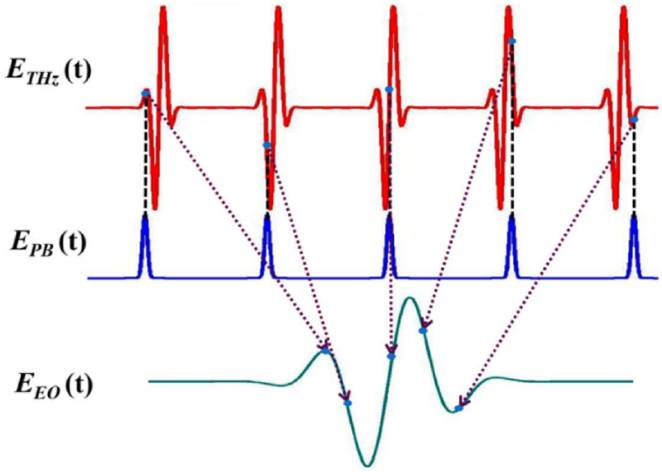

Figure 5.2: From [11]. Electric Field trace reconstruction by electro-optic sampling.

prieties, e.g. dispersion and absorption inside the crystal and at the interfaces, Fabry-Perot effects inside the crystal. Once again the crystal of choice was GaSe, since not only has a sufficiently large electro-optic coefficient, but, if thin enough, it ensures a good transparency, low dispersion and good velocity matching of probe and THz beam.

There is, anyway, a fundamental requirement for the EOS to work efficiently, that is entirely connected to the probe, and that is the time duration of the latter. Indeed, if it is not short enough, the quasi DC approximation of the Mid-IR does not hold anymore and the pulse mapping, when feasible, is not reliable. Usually a small fraction[5] of the amplified beam coming out of the Ti:Sa laser is used as gating pulse. In our case this was not possible since we choose the time duration of the amplifier pulse to be quite long to optimize the OPA processes. Indeed that was 90 fs, which is three times longer than the period of a 30 THz (10 μm) pulse and almost twice the period of a 20 THz (15 μm) pulse.

[5]The probe power needs to be detectable but low enough to avoid any unwanted non-linear effect.

The idea was then to use a small part of the oscillator beam, which has a time duration of roughly 13 fs, as gating pulse. This was a challenge since the repetition rate of the oscillator and of all the rest of the system are different, respectively 80 MHz and 1 KHz. The solution was to use a fast balanced detector and really fast oscilloscope to find the only pulse of the oscillator's train traveling inside the crystal at the same time as the THz out of the other 79999 that were not, and then use a Boxcar Averager (BA) beside the usual Lock-In Amplifier (LIA). The lock-in amplifier is used to extract the tiny signal we are interested in out of the noise. This works by chopping the signal we want to acquire (which is the Mid-IR in this case), so that it becomes modulated at a well know frequency determined by the angular velocity of the blades of the chopper. The difference signal is then demodulated and low pass filtered so that the flickering noise is suppressed. The boxcar works before the demodulation and filtering of the Lock-In and it is used to gate and extract the single pulse we want out of the train of pulses coming from the oscillator which do not correspond to any Mid-IR pulse.

The final results were excellent. Indeed lots of the Electric Field traces displayed in the Thesis were acquired with this system, which has intrinsically a high time resolution[6] and moderately high signal to noise ratio (depending almost entirely on the goodness of the system's alignment).

5.2 Active Stabilization

Theoretically speaking, passive stabilization described in the previous chapter should be already enough to guarantee the CEP stability. In fact the DF mixing of two mutually phase-locked pulses generate a intrinsically phase stable train of pulses. This technique, however, requires high stability of the path lengths of the two interacting beams, since even a little delay between the two produce a

[6]The time resolution is actually only limited by the spatial resolution achievable in delaying the probe beam in respect to the THz pulse, which is usually quite high.

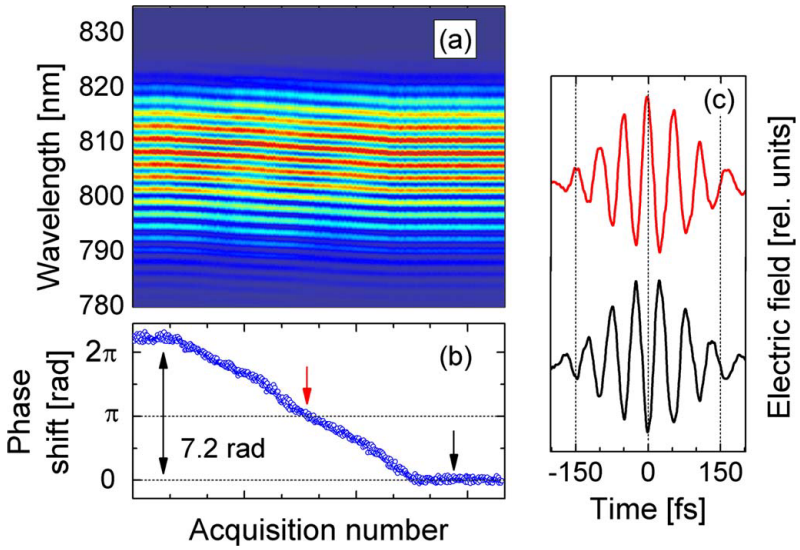

Figure 5.3: From [1]. (a) Sequence of spectra acquired during the introduction of 3.5 μm of fused silica glass on the pump beam path and (b) corresponding phase shift. (c) Electric field deduced from EO sampling of the MIR pulses for the two phase values indicated by the arrows in panel (b).

phase shift in the resulting Mid-IR beam. Typically temperature or mechanical fluctuations and long-term drifts are mainly responsible for this relative delays and they are usually really difficult to eliminate. To react to this problems active stabilization is needed, especially on the long-term drifts that we must avoid in order to be able to run experimental measurements lasting up to several days.

The active stabilization consists in reading the phase information and then actively change the path length of one of the two beams in order to compensate for the unwanted delay. The path length correction on our setup is performed by inserting a fused-silica wedge pair on the path of one of the beams[7]. One of the two wedges can be moved in, or out, changing the thickness of material that the light passes through, hence changing the delay of that beam in respect to the other. The movable wedge is mounted onto a high-resolution stepper motor assuring a really good control over the delay and therefore on the phase, as one

[7]This is done when the NIR is not too intense to avoid any nonlinearities, so before the second stage amplification.

can see from Figure 5.3.

To control the phase drifts it necessary to detect them quite carefully. There are various systems that can be used for this purpose but we will mention here just the two that are in use in our labs. They are both based upon the same principle, which is mixing the Mid-IR pulse and a gate pulse, but one works in frequency domain, while the other in time domain. Both the techniques can work in parallel to the main experiment, indeed for the detection and correction of the phase just a relatively small amount of power of Mid-IR is needed. For such reason, when the experiments are running a beam splitter divides a minor part of the beam towards the detection, leaving all the rest available to the experimental setup. The frequency-domain measurement system had already been demonstrated [1] to work effectively and reliably while the time-domain one was, at the time we approached it, just been proposed. Indeed, one of the main goals of the author's experience in the labs was to prove the time-domain active stabilization, setting up all the necessary tools and optics and working on the control software. The idea was then to compare the results of the two systems and see which one was to be preferred, and in which case should one consider using the time-domain instead of the frequency-domain.

The frequency-domain technique consist in DF mixing the Mid-IR and a optical gate pulse (typically an 800 nm source) so that the resulting DF field will then give rise to fringe pattern by spectral interfering with the gate pulse. In fact the DF pulse have an absolute phase of:

$$\phi_{DF} = \phi_{Gate} - \phi_{MIR} - \pi/2 \tag{5.8}$$

Hence the phase ϕ of the fringe pattern in the frequency domain will be:

$$\phi = \phi_{gate} - (\phi_{Gate} - \phi_{MIR} - \pi/2) + const. = \phi_{MIR} + const. \tag{5.9}$$

Therefore, measuring with a spectrometer the fringe pattern one can retrieve the absolute-phase drift of the Mid-IR independently from the CEP of the gate pulse. A typical example of interference pattern is displayed in Figure 5.4. The DFG process is performed in a 50 μm thick GaSe crystal adjusted for Type II interaction [e(MIR)+e(Gate)→o(DF)] so the resulting co-propagating gate and DF pulses are cross-polarized. They are then relatively delayed by a 2 mm thick α-barium borate plate, projected to the same polarization[8] before being directed onto the spectrometer. In this way the CEP can be maintained stable over hours

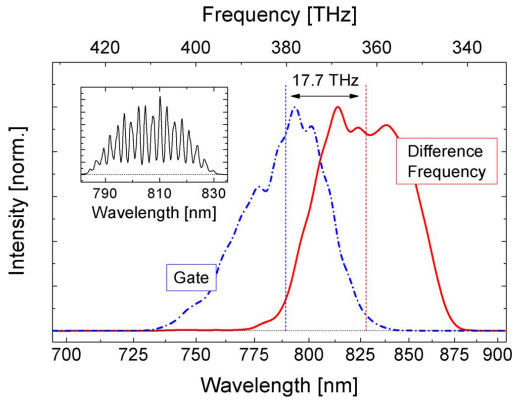

Figure 5.4: From [1]. Spectra of the gate (blue dashed-dotted line) together with the side band (red solid line) arising from difference frequency mixing with the MIR pulses in a GaSe crystal. Inset, fringe pattern from balanced spectral interference between gate and DF pulses.

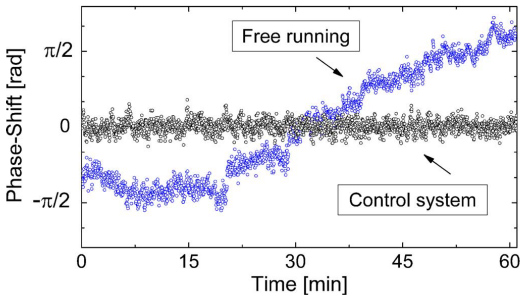

Figure 5.5: From [1]. Long-term characterization of the MIR phase drift. Both free-running and closed loop measurements are displayed.

of operation. In Figure 5.5 there is a comparison between the phase drift of the Mid-IR when the active stabilization is on against when it is off. It is easy to

[8]With an achromatic polarizer.

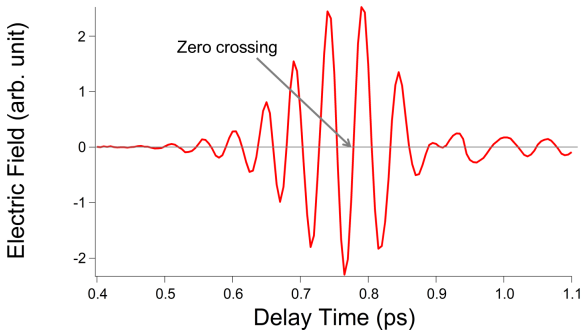

Figure 5.6: EOS of a pulse and chosen zero crossing point for the stabilization.

see that the short-time fluctuations are present in both the situations while the long-term drift is perfectly corrected with the control system on. This ensures a good enough pulse and strong stability to work with for the experiments.

Although the frequency-domain measurement leads to good control over the system CEP stability it can not work in our setup, as it was initially designed. Indeed it needs a broad enough 800 nm gating pulse, actually broader than the Mid-IR carrier frequency, which, in time domain, means having the time duration shorter than one Mid-IT optical cycle. This is not the case, as one may recall, of our amplified beam[9]. Hence we decided to use the oscillator instead, but, since the repetition rate is too high for the spectrometers to properly work we turned into time domain. The equivalent of the above describe measurements' setup in the time domain is the EO sampling apparatus.

The EO sampling can be used as follows. The first thing is to run a trace acquisition of the Mid-IR, then a zero-crossing point can be chosen from the trace, upon which the stabilization will take place (Figure 5.6). It is better to choose one of the steep zero crossings near the center of the pulse, since it gives more sensibility, and, at the same time, better signal to noise ratio. The motorized stage on the probe pulse is moved so that the delay is such that the sampling correspond to

[9]Which is 90 fs so too long, i.e. too narrow in the spectral domain.

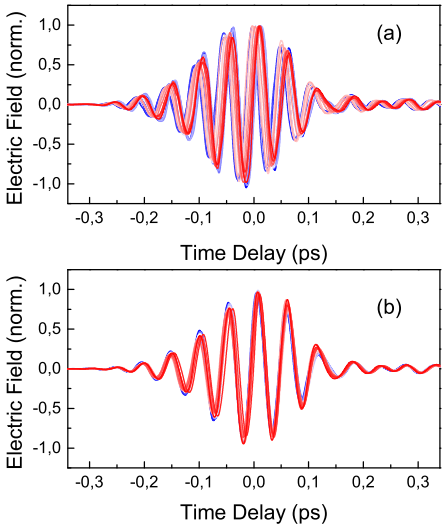

Figure 5.7: 20 different EOS traces acquired over the course of one hour with active stabilization off (a) and on (b). The traces go from blue to red with the time.

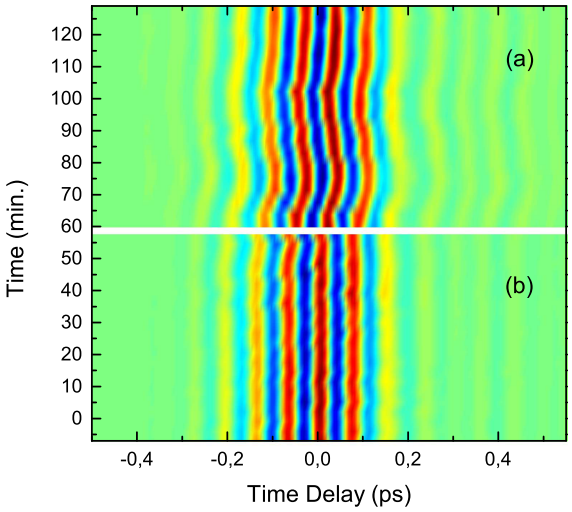

Figure 5.8: Sequence of traces acquired over the course of one hour showing the phase shifting of free running (a) and actively stabilized (b) pulses. It can be imagined as the top view of the Figure 5.7 as the time passes.

the chosen zero crossing point. Now the setup is ready to run the stabilization. This is done by reading the intensity of the electric field, if it is zero this means that the CEP is stable, if it goes up or down it means that the pulse is "shifting" to the left or the right, but, since the delay time are locked, this implies that the phase is changing. If the phase is drifting the computer program can hence react moving the fused-silica wedge to compensate for the drift. The measurement is, of course, affected by some noise and errors so there is a filter that average over some time before moving the stage to avoid overshooting of the feedback loop. The final result is displayed in Figure 5.7 and Figure 5.8.

This traces were measured in parallel to the stabilization with a second EO sampling mounted in the place of the experimental setup. In Figure 5.7 (b) it is clear that the actively stabilized pulses are almost perfectly on top of each other, so with an almost perfect CEP stability. The Figure 5.8 (b) once again confirms this sensation; the central peaks in red are really straight meaning the the CEP

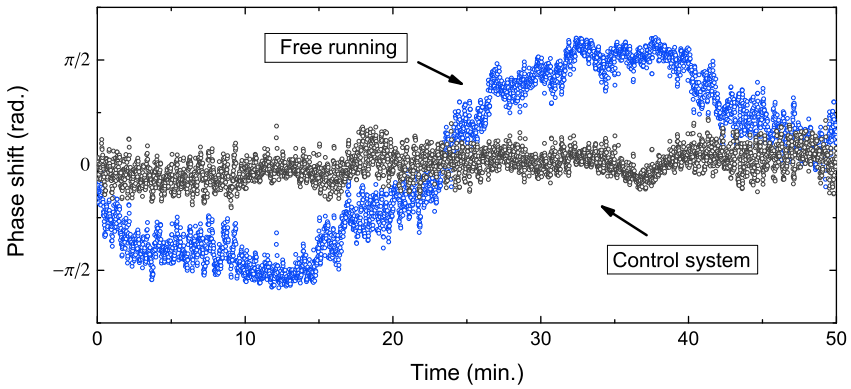

Figure 5.9: Long-term characterization of the MIR phase drift. Both free-running and time-domain stabilized measurements are displayed.

is not changing. On the other hand, it is just as much obvious from both the figures (5.7(a),5.8(a)) that the free running traces swing left and right quite a lot. Looking in particular at Figure 5.7 (a) it is reasonable to think that, as the time goes by, they will eventually form an indistinguishable candy-shaped blob from which the phase information would be impossible to retrieve. This is a visual confirmation of the importance of the CEP stability for phase sensitive processes.

As above discussed, to our system, as it is, the frequency-domain technique can not be applicable. It could be anyway modified to work also in the frequency-domain by compressing the laser pulse and use that as a gate. At this point one might wonder which of the two methods should be used, and why. In Figure 5.9 is displayed the corresponding graph of Figure 5.5 to compare the performances of the techniques. The difference is minimal, as it should be, since the physical phenomenon on which both rely on is the same. One might argue that both "curves" in the time-domain graph looks a bit thicker in respect to the frequency-domain ones. This is not caused by the feedback loop of course, otherwise the free-running would be thinner than the stabilized one, which is not the case. Indeed, doing the calculations it turns out that the standard deviation of the two different actively

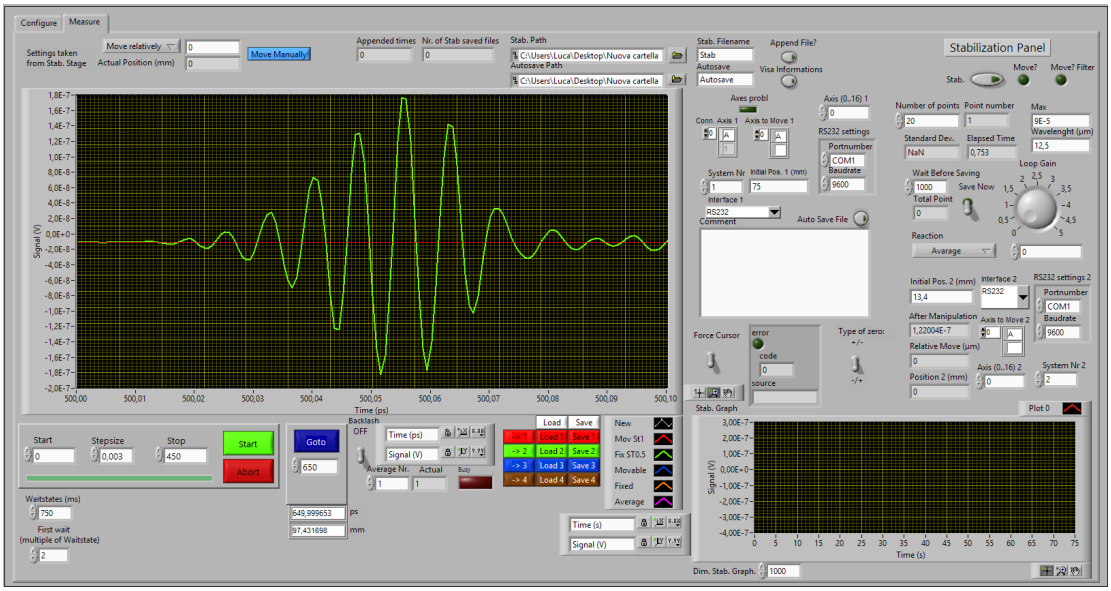

Figure 5.10: Screen shot of the main panel of the EOS and stabilization controlling program.

stabilized methods is practically the same (115 mrad against 110 mrad[1]). So the results are actually really analogous and the only differences are in the plotting and in the number of points that create the artificial sensation of discrepancy. It is important to notice, anyway, that none of the two methods can compensate for fast jitter[10]. All considered, this is almost irrelevant and therefore both can equivalently be used in stabilization with no particular concerns.

One of the most crucial part of the whole system was the computer program that took care of the detection as well as the stabilization. It is important since it interacts with all the stages and detection electronics to keep the system working and the phase stable. Many different algorithms were implemented to properly feedback loop the system, but in the end we decided for one of the most trivial since it was anyway quite accurate and really reliable. Not only to give credit to its importance but also to show the actual complexity of such tools there is a screen shot of the main panel of the just mentioned computer program in Figure 5.10.

[10]The main problem is the presence of measurement noise that cannot really be distinguished from the fast jitter.

5.3 MidIR Narrowband

Some experiments call for an higher control on the spectral content of the Mid-IR, some need broader spectra, others ask for narrower, others still request a particular shaped spectrum. We were interested in finding a way to obtain a narrow-band Mid-IR. One can come up with lots of ideas on how to use this kinds of pulses in many different experiments related to many more diverse fields. Anyway, usually a narrow-band pulse is useful either, to make sure to hit the sample with the right frequency to pump the needed excitation and nothing else, either, to probe strictly in the region of interest and nowhere else.

The Mid-IR pulses generated in our setup have typically a spectral width around 10% of the frequency, so for 20 THz approximately 2 THz, which is not really broad, neither really narrow. To obtain narrower spectra one can make use of a quite simple, but really clever, technique which is enlighten in Figure 5.11. Two

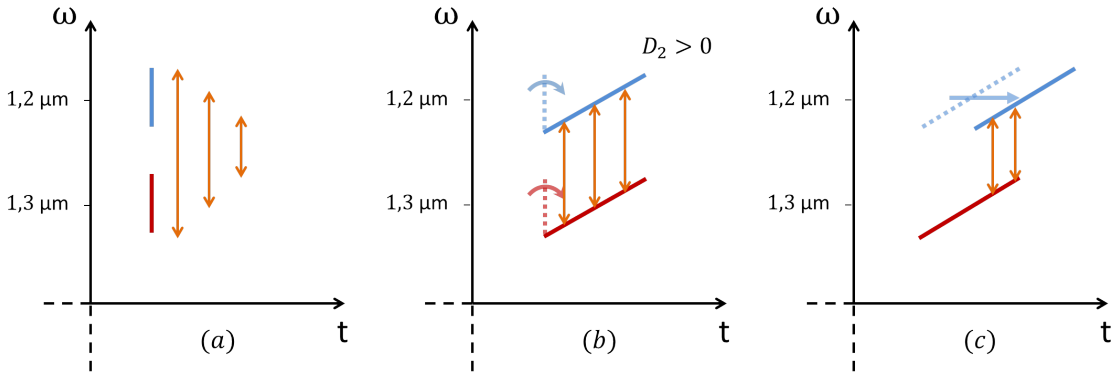

Figure 5.11: Intuitive explanation of narrow-band Mid-IR generation. In blue a NIR centered around 1.2 μm and in red one centered around 1.3 μm. The orange arrows represent the difference frequency value, which will be the Mid-IR's spectrum. (a) Two ideal unchirped pulses (b) the pulses get positively chirped into a crystal (c) the chirped pulses are shifted reciprocally in time.

ideal NIR pulses are displayed in Figure 5.11 (a). Since they are unchirped, all the

frequencies arrive at the same time[11] and hence there are quite a few difference combinations available. This means that, in this case, the generated DF Mid-IR will have a reasonably broad spectrum, limited mostly by the width of the NIR spectra and slightly by the phase matching angle of the generation crystal[12]. This is basically what happens normally for the Mid-IR generation on our setup.
If the pulses get equally linearly chirped[13] the frequencies become spread out along the pulse, and the pulse itself gets longer as shown in Figure 5.11 (b). For these reasons, as the pulses pass inside the generation crystal the possible combinations of difference frequency are really limited. This means that the Mid-IR will have a quite narrow spectrum and, at the same time, a long time duration.
With such chirped NIRs, shifting one of the two in time intrinsically means changing the frequency of the Mid-IR as displayed in Figure 5.11 (c). This because we combine two part of the Mid-IR Spectra that before were not interacting. This is, not only a good proof of the proper functioning of the technique, but also a possible alternative to reach frequencies otherwise difficult to obtain. The counterpart of this last approach is that some part of the spectrum, hence the power, get lost due to the detuning.
The trickiest part of this process is the chirping: it has to be quite relevant, yet, at the same time, identical for the two NIR and almost perfectly linear[14]. For the purpose three 5 cm thick ZnSe crystal were placed on each NIR pulse's path. Those have been carefully chosen to have an almost perfect linear dispersion around the frequencies of interest, good transmission and low imperfections. Since they must be placed after the second stage of OPA to be effective, the two beams needed to be telescoped to enlarge their size in order to avoid any unwanted non-linear effect. Despite all these careful precautions, the fact that the

[11] Limited just by the bandwidth-time dichotomy.
[12] As we saw, the PM condition is not really so stringent.
[13] Positive chirp is the most frequent, but the arguments are valid also with negative chirp.
[14] Meaning that the time-frequency graph must be linear, hence only with GVD and v_g different than zero.

NIR beams have to pass trough a lot of optics causes their power to drop of about 10%, which is anyway quite a good result[15]. Despite that, the final efficiency of the setup is quite lower compared to the broadband one. This is totally normal; indeed having longer NIRs pulses means that their peak-intensity is lower than equally powerful pulses, therefore the non-linear effects, DFG included, become less efficient. Instead the spectra looks just the same, as it should be, proving that no strange effects are present.

If everything is done right then the result can be quite good, as displayed in Figure 5.12. In green we plotted data obtained with a normal setup, while in blue the same data obtained with the narrow-band setup, basically the difference is just the addition of the ZnSe crystals. In Figure 5.12 (a) we can appreciate the effect above described: the spectrum of the Mid-IR change drastically from a FWHM of approximately 2,5 THz (10%[16]) to 0.5 THz (less than 2%). This is a remarkable narrowing which can be useful for many experimental applications. Nevertheless, one may notice that the central frequency is shifted from 26 to roughly 27,5 THz, this was expected both by the theoretical description and by some experimental details. The spectra can be overlapped, if needed, tuning the narrow-band PM angles as well as the OPAs[17], but we decided to keep the things as simple and clear as possible to demonstrate the capabilities of this system. In Figure 5.12 (b) are displayed the envelopes of the two pulses. As expected the narrow one is longer (0,76 against 0,32[18] ps) which can be useful as well, in some experiments. Here the temporal shifting is totally artificial, it was just inserted for aesthetic reasons. One nice thing that can be noticed is the similarity of the spectrum of the narrow-band pulse with the envelope of the broad-band one and vice-versa;

[15] A loss of 10% is in perfect agreement with the optics figures.

[16] This percentages are referred, as before, to the central frequency.

[17] As one can see from Figure 5.11 the DF change from (a) to (b), so to obtain the same frequency tuning of the OPAs is needed.

[18] FWHM value.

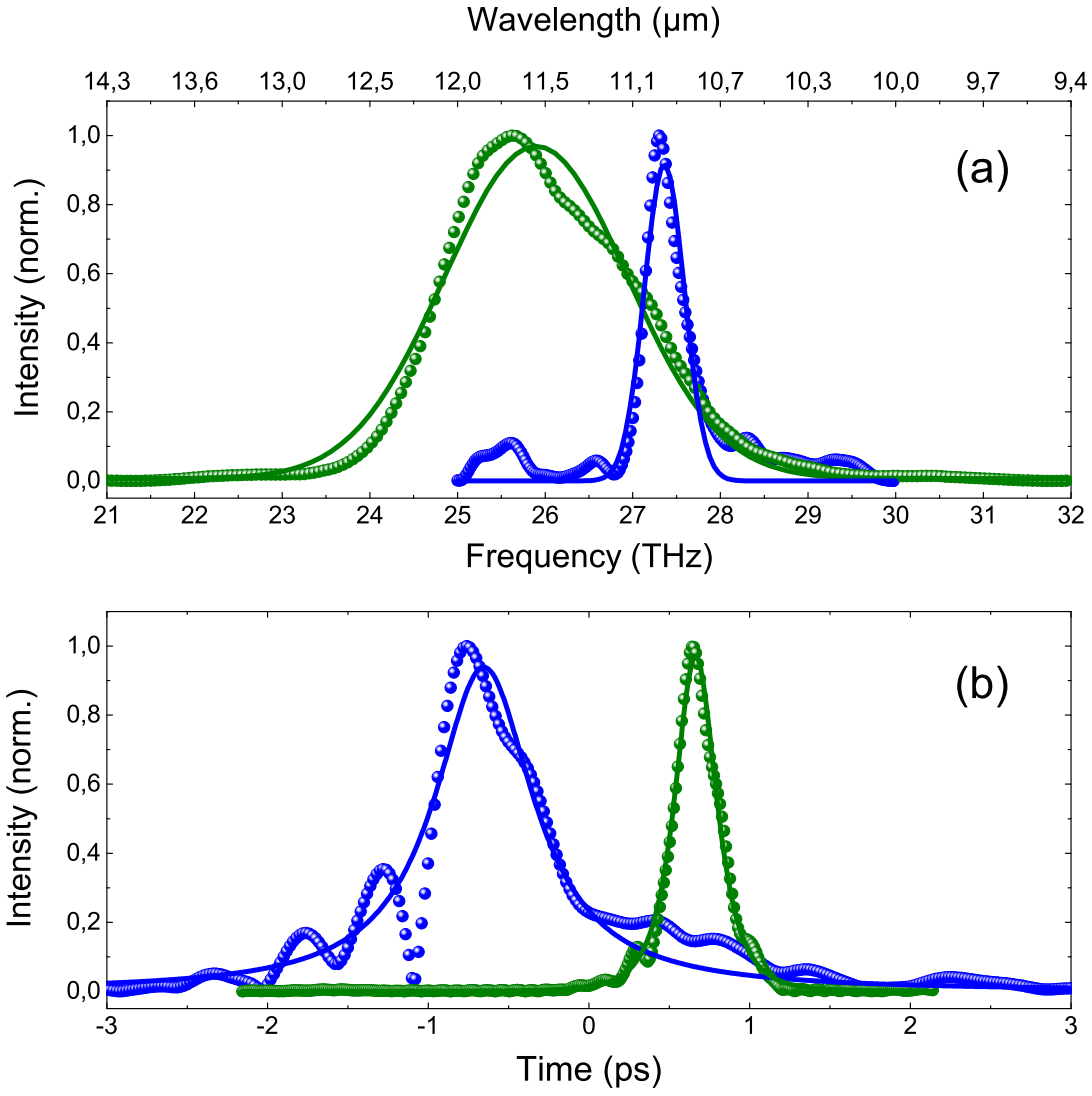

Figure 5.12: (a) Mid-IR spectra of narrow (blue) and broad (green) band pulses. (b) Mid-IR envelopes of the narrow (blue) and broad (green) band pulses. The solid lines are fitting of the dots, which are data.

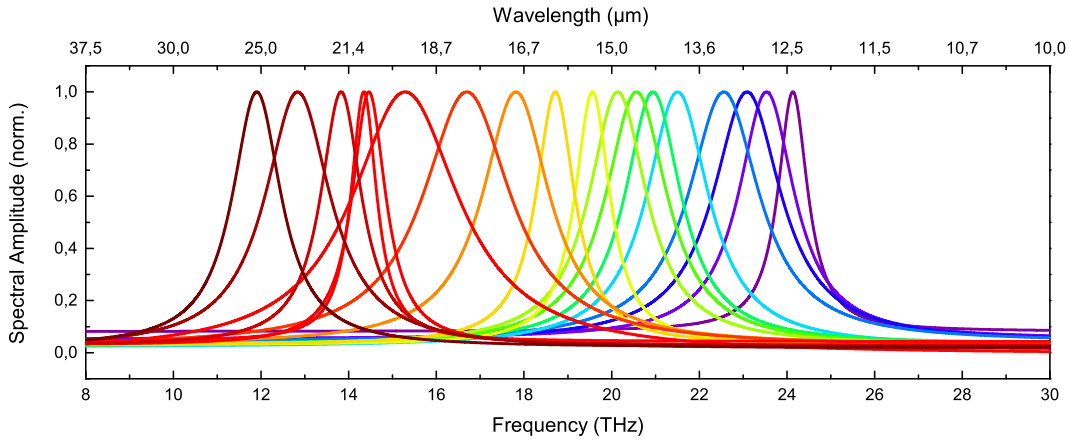

Figure 5.13: Spectra of Mid-IR pulses acquired with different time delay between the NIR beams generating the Mid-IR.

this is partially due to some artificial casualties in the plotting, but partially to the frequency-time dichotomy. Again, as previously mentioned, the power loss means that the data from the narrow-band pulses looks more noisy. This is also partially due to the less knowledge on the behaviors of the latter in comparison to the fully characterized broadband.

To check that we were doing it right we decided to detune the time delay of the NIRs in the narrow-band setup to reconstruct the situation of Figure 5.11 (c). The result in Figure 5.13 and Figure 5.14 show good agreement with the expected behavior. The Figure 5.14 shows the dependence of the generated frequency/wavelength upon the detuning of the time delay of the pulses. What was predicted from the theoretical arguments still applies to the behavior shown in the plot: the more the pulses are shifted in time the more the difference frequency change. And this is also clear from Figure 5.13 in which we see the fittings of the spectra of narrow-band Mid-IR as the time delay is detuned. It might appear that some of the spectra are actually quite broad, this can be ascribed to various different reasons. First of all the power loss due to the detuning is quite relevant, hence the signal to noise ratio of some of the spectra is quite poor and

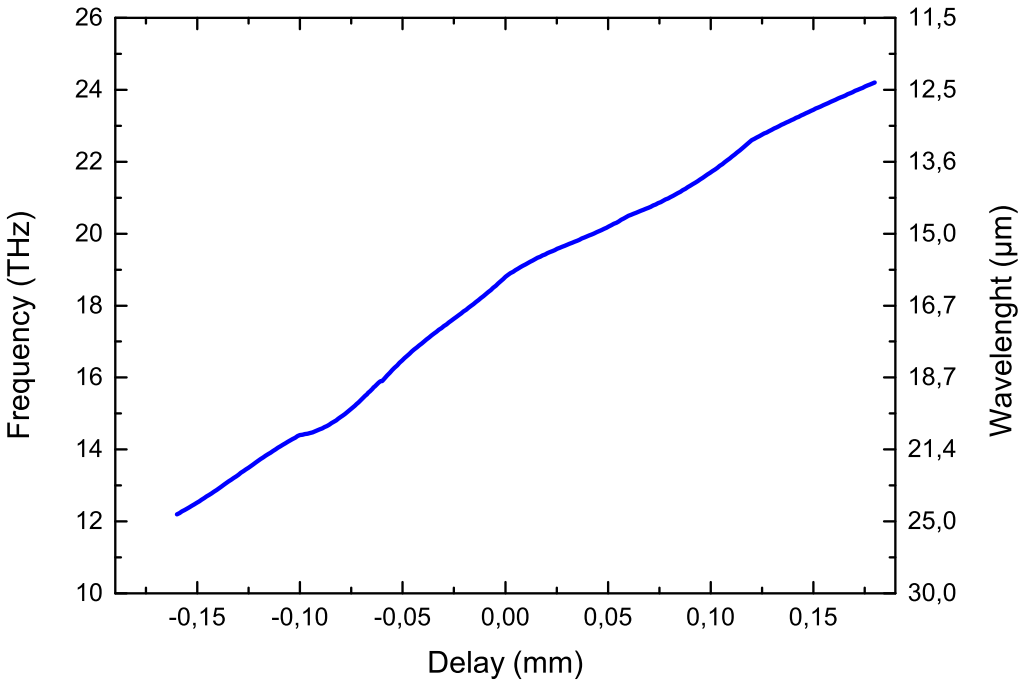

Figure 5.14: Central frequency and wavelength of Mid-IR pulses generated as the delay between the NIR beams is changed.

that can cause a wrong fitting especially concerning the FWHM. Since it was just a check test we did not have time to fully optimize every pulse, and moreover the optimization could also mean messing up the test. The normalization and fitting of the spectra that were needed to show a readable graph could dramatize a bit the already existing differences. Nevertheless the global result is good and the technique seems to be really promising and quite reliable.

Chapter 6

Results and Conclusions

The overall description of the building and characterization of a CEP stable Mid-IR source has been given. The frequency generated by the setup can be tuned between 15 THz (20 μm) and 30 THz (10 μm), with resulting average power over 6 mW (6 μJ at 1 KHz). The detection setup has been introduced and it has been demonstrated to be working, even with the unusual use of the oscillator as probing pulse. Newly proposed active stabilization of the setup in time-domain has been proved to be effective and to be performing comparably with the already established frequency-domain method[1]. Finally, narrow-band Mid-IR generation through chirped NIR difference frequency mixing has been intuitively explained and then confirmed by measurements and data that show some promising features. Both time-domain active stabilization and Mid-IR narrow-band generation should be considered for stable future implementation.

Bibliography

[1] C. Manzoni, M. Först, H. Ehrke, and A. Cavalleri, "Single-shot detection and direct control of carrier phase drift of midinfrared pulses," *Optics Letters*, vol. 35, no. 5, pp. 757–759, 2010. [Online]. Available: http://www.opticsinfobase.org/ol/abstract.cfm?URI=ol-35-5-757

[2] M. Caorsi, "Principi ed applicazioni dei laser," 2010.

[3] C. Rullière, *Femtosecond Laser Pulses*. Springer, 2005.

[4] M. Perry, B. Shore, R. Boyd, and J. Britten, "Multilayer dielectric gratings: Increasing the power of light," *Science & Technology Review (LLNL)*, 1995. [Online]. Available: https://str.llnl.gov/str/pdfs/09_95.2.pdf

[5] G. M. Rossi, *Generation Of Broadband Mid-Infrared And Ultraviolet Pulses From Optical Parametric Amplifiers*. Politecnico di Milano, 2013.

[6] G. Cerullo, A. Baltuška, O. Mücke, and C. Vozzi, "Few-optical-cycle light pulses with passive carrier-envelope phase stabilization," *Laser & Photonics Reviews*, vol. 5, no. 3, pp. 323–351, 2011. [Online]. Available: http://dx.doi.org/10.1002/lpor.201000013

[7] B. Mellish. [Online]. Available: http://en.wikipedia.org/wiki/Self-phase_modulation

[8] E. Optics. [Online]. Available: http://eksmaoptics.com/out/pictures/master/product/11/gasetransmission.jpg

[9] F. Junginger, A. Sell, O. Schubert, B. Mayer, D. Brida, M. Marangoni, G. Cerullo, A. Leitenstorfer, and R. Huber, "Single-cycle multiterahertz transients with peak fields above 10 MV/cm," *Optics Letters*, vol. 35, no. 15, pp. 2645–2647, Aug 2010. [Online]. Available: http://ol.osa.org/abstract.cfm?URI=ol-35-15-2645

[10] C. O'Sullivan and J. A. Murphy, *Terahertz Sources, Detectors, and Optics*. John E. Greivenkamp, SPIE Press, 2012.

[11] A. Tomasino, A. Parisi, S. Stivala, P. Livreri, A. C. Cino, A. C. Busacca, M. Peccianti, and R. Morandotti, "Wideband thz time domain spectroscopy based on optical rectification and electro-optic sampling," *Scientific Reports*, vol. 3, no. 3116, 2013. [Online]. Available: http://dx.doi.org/10.1038/srep03116L3

[12] R. W. Boyd, *Nonlinear Optics*. Elsevier Inc., 2008.